PHILOSOPHICAL TRANSACTIONS OF THE ROYAL SOCIETY A MATHEMATICAL, PHYSICAL & ENGINEERING SCIENCES

Experimental Chaos from Autonomous Electronic Circuits

Michael Peter Kennedy

Phil. Trans. R. Soc. Lond. A 1995 **353**, 13-32
doi: 10.1098/rsta.1995.0087

Experimental chaos from autonomous electronic circuits

By Michael Peter Kennedy

Department of Electronic and Electrical Engineering, University College Dublin, Dublin 4, Republic of Ireland

Autonomous electronic circuits provide a convenient framework in which to study chaotic phenomena. These systems are easy to build, easy to measure, and easy to model using differential and difference equations. Furthermore, they operate in real time, and parameter values are readily adjusted.

In this work, we discuss the nature of chaotic steady-state behaviour and describe how it manifests itself in autonomous electronic circuits. We study state space, time- and frequency-domain measurement techniques for characterizing steady-state behaviour. Because of its value as a paradigm for exploring chaos, we choose Chua's oscillator as the vehicle for our experiments.

1. Introduction

DC equilibrium, periodic, and quasi-periodic steady-state solutions of electronic circuits have been correctly identified and classified since the pioneering days of electronics in the 1920s. By contrast, the existence of chaos has only been widely acknowledged in the past 30 years.

Even though the notion of chaotic behaviour in dynamical systems has existed in the mathematics literature since Poincaré's work at the turn of the century, unusual behaviour in the physical sciences as recently as the 1970s was being described as 'strange' (Ruelle & Takens 1971). Today, we classify as *chaos* bounded recurrent motion in a deterministic dynamical system which is characterized by sensitive dependence on initial conditions (Thompson & Stewart 1986; Ott 1993).

Although the future behaviour of a chaotic system is determined exactly by the initial conditions, sensitive dependence on initial conditions means that the precision with which these conditions must be specified grows exponentially with the length of the prediction. Thus, a real chaotic system appears to exhibit 'randomness' in the time domain because its initial conditions cannot be specified with sufficient precision to make accurate long-term predictions of its behaviour.

The earliest experimental observations of chaos in electronic circuits were in forced nonlinear oscillators, including the sinusoidally excited neon bulb relaxation oscillator studied by van der Pol & van der Mark (1927) and Kennedy & Chua (1986), the forced negative-resistance oscillator of Ueda & Akamatsu (1980) and the driven series-tuned RL-diode circuit (Linsay 1981; Testa *et al.* 1982). More recently, chaos has been observed and studied in a variety of unforced *autonomous* electronic circuits.

In this work, we discuss the nature of chaotic steady-state behaviour and describe how it manifests itself in real electronic circuits.

Phil. Trans. R. Soc. Lond. A (1995) **353**, 13–32
Printed in Great Britain

2. Autonomous electronic circuits

A *lumped* electronic circuit (one whose physical dimensions are small compared to the wavelengths of its voltage and current waveforms (Chua *et al.* 1987)) containing resistive elements (resistors and voltage and current sources) and n independent energy-storage elements (capacitors and/or inductors) can be described by a system of ordinary differential equations (called *state equations* (Chua *et al.* 1987)) of the form,

$$\dot{\boldsymbol{X}}(t) = \boldsymbol{F}(\boldsymbol{X}(t), t),$$

where $\boldsymbol{X}(t) = (X_1(t), X_2(t), \ldots, X_n(t))^{\mathrm{T}} \in \mathbb{R}^n$ is called the *state vector* and $\boldsymbol{F}$ is called the *vector field*. $\dot{\boldsymbol{X}}(t)$ denotes the derivative of $\boldsymbol{X}(t)$ with respect to time.

If the vector field $\boldsymbol{F}$ depends explicitly on t, then the system is said to be *non-autonomous*. Non-autonomous electronic circuits are discussed in the paper by Lakshmanan in this volume. If the vector field depends only on the state and is *independent* of time t, then the system is said to be *autonomous* and may be written in the simpler form:

$$\dot{\boldsymbol{X}} = \boldsymbol{F}(\boldsymbol{X}). \tag{2.1}$$

In this work, we focus exclusively on *autonomous* electronic circuits. The time evolution of the state of an autonomous electronic circuit from an initial point $\boldsymbol{X}_0$ at $t = 0$ is given by

$$\boldsymbol{\phi}_t(\boldsymbol{X}_0) = \boldsymbol{X}_0 + \int_0^t \boldsymbol{F}(\boldsymbol{X}(\tau))\,\mathrm{d}\tau, \quad t \in \mathbb{R}_+,$$

where $\boldsymbol{\phi}_t : \mathbb{R}^n \to \mathbb{R}^n$ is called the t-advance map. $\boldsymbol{\phi}_t$ takes state $\boldsymbol{X}$ to state $\boldsymbol{\phi}_t(\boldsymbol{X})$ t seconds later. The solution $\boldsymbol{\phi}_t(\boldsymbol{X}_0)$ is called a *trajectory* through $\boldsymbol{X}_0$, and the set $\{\boldsymbol{\phi}_t(\boldsymbol{X}_0), t \in \mathbb{R}_+\}$ is an *orbit* of the system (2.1). The collection of maps $\{\boldsymbol{\phi}_t\}$, which describe the evolution of the entire state space with time, is called the *flow*.

(*a*) *Steady-state solutions*

An autonomous electronic circuit is an example of a *deterministic dynamical system*. A *deterministic* dynamical system is one whose state at any time is *completely determined* by its initial state and the rule (called its *dynamic*) which determines the time evolution of its state space. Here, the initial state is $\boldsymbol{X}_0$, the dynamic is $\dot{\boldsymbol{X}} = \boldsymbol{F}(\boldsymbol{X})$, and the state at any time t is given by $\boldsymbol{X}(t) = \boldsymbol{\phi}_t(\boldsymbol{X}_0)$.

From a given initial state, a trajectory of a dissipative circuit wanders through the state space, asymptotically approaching a region of the state space called a limit set. (A dynamical system (2.1) is said to be *conservative* if $\nabla \cdot \boldsymbol{F}(\boldsymbol{X}) = 0 \,\forall\, \boldsymbol{X}$ and *dissipative* if $\nabla \cdot \boldsymbol{F} < 0$ in some region of the state space (Ott 1993). Dissipation enables trajectories to converge asymptotically towards limit sets in forward time. Real electronic circuits are normally dissipative due to heat loss in positive-valued resistors.) In the limit set, the system exhibits *steady-state* behaviour. An *attracting limit set* (more commonly called an *attractor*) is a set of states to which nearby states evolve in forward time. In an experiment, only *attracting* steady-state solutions can be observed. Therefore, the steady-state behaviour of a real circuit corresponds to motion on an attracting limit set. Because of the experimental focus of this work, we consider only attracting limit sets.

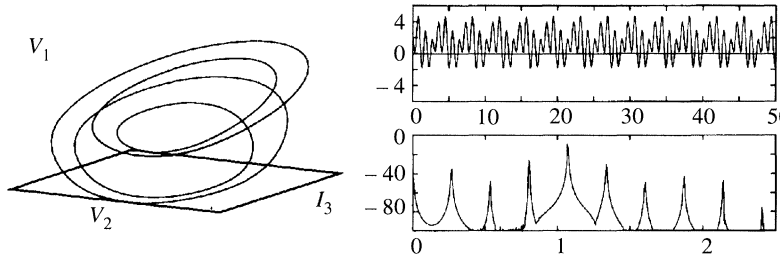

Figure 1. Simulated state space trajectory, time waveform, and power spectrum for Chua's oscillator (see § 4). Periodic steady-state, all spikes in the power spectrum are harmonically related to the fundamental frequency. Time plot: horizontal axis, t (ms); vertical axis, $V_1(t)$ (V). Power spectum: horizontal axis, frequency (kHz); vertical axis, power of $V_2(t)$ (dB).

(i) *DC solution*

The simplest type of limit set is an *equilibrium point* (also known as a *stationary point* or a *fixed point*), which corresponds to a DC solution of a circuit. $\boldsymbol{X_Q}$ is an equilibrium point of (2.1) if $\boldsymbol{F}(\boldsymbol{X_Q}) = 0$. Equivalently, $\boldsymbol{\phi}_t(\boldsymbol{X_Q}) = \boldsymbol{X_Q} \forall t$.

(ii) *Periodic solution*

A state $\boldsymbol{X}$ of the dynamical system (2.1) is called *periodic* if there exists $T > 0$ such that $\boldsymbol{\phi}_T(\boldsymbol{X}) = \boldsymbol{X}$. A periodic point which is not an equilibrium point is called a *cycle*. A *limit cycle* is an *isolated* periodic solution; in state space the orbit corresponding to a limit cycle trajectory is a simple closed curve $\Gamma \subset \mathbb{R}^n$.

Since a limit cycle trajectory visits each point on Γ with period T, the n component waveforms $X_i(t)$ of this trajectory are periodic with period T.

If the vector field of an autonomous electronic circuit is a *continuous* function of the state (as is typical in real electronic circuits), then no trajectory of the system may go through the same point twice in two different directions. In particular, no two trajectories may *cross each other*; this is called the *non-crossing property* (Thompson & Stewart 1986).

The implication of this is that a second-order autonomous circuit (whose trajectories lie in the plane) can exhibit just two types of steady-state behaviour: an *equilibrium point* or a *limit cycle* (Vidyasagar 1978). An autonomous circuit containing just two energy-storage elements cannot produce a steady-state behaviour which is more complicated than this. In particular, a continuous system described by an autonomous second-order differential equation cannot exhibit chaos; for that, three differential equations are required.

(iii) *Quasi-periodic solutions*

While a three-dimensional state space is *necessary* to produce chaos in an autonomous continous-time circuit, it is not sufficient. Another form of steady-state behaviour which can occur in a state space of dimension greater than two is *quasi-periodicity.*

A quasi-periodic function is one which may be expressed as a countable sum of periodic functions with incommensurate frequencies, i.e. frequencies which are not rationally related. For example $X(t) = \sin(t) + \sin(2\pi t)$ is a quasi-periodic signal. In

PHILOSOPHICAL TRANSACTIONS OF THE ROYAL SOCIETY A MATHEMATICAL, PHYSICAL & ENGINEERING SCIENCES

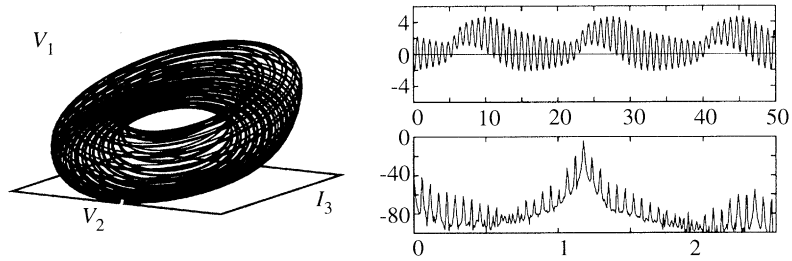

Figure 2. Simulated state space trajectory, time waveform, and power spectrum for Chua's oscillator (see § 4). Quasi-periodic steady-state, discrete power spectrum with incommensurate frequency components. Time plot: horizontal axis, t (ms); vertical axis, $V_1(t)$ (V). Power spectrum: horizontal axis, frequency (kHz); vertical axis, power of $V_2(t)$ (dB).

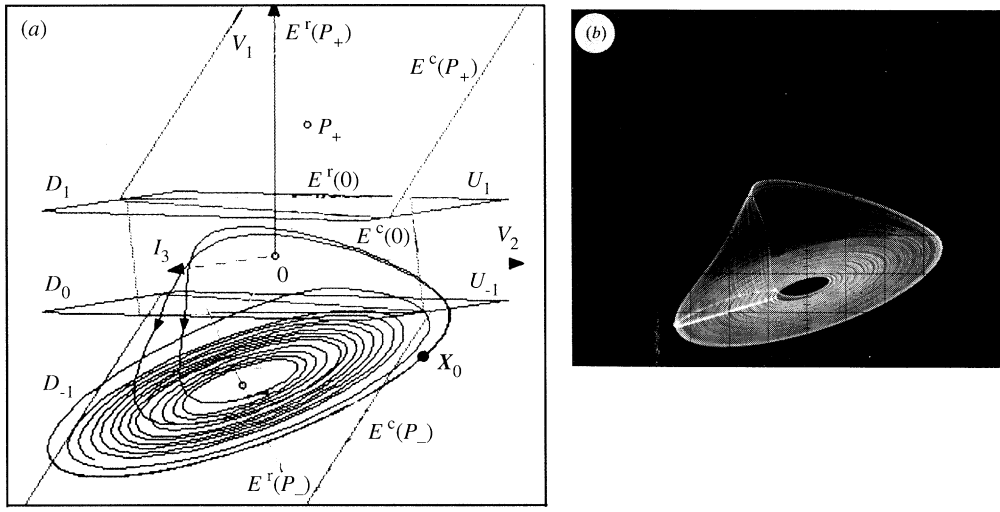

Figure 3. Stretching and folding mechanism of chaos generation in Chua's oscillator (see § 4). (*a*) Simulated spiral Chua chaotic attractor showing affine regions (D_{-1} and D_1), separating planes (U_{-1} and U_1), equilibrium points ($P_-, 0$, and P_+), and their associated eigenspaces (E^r and E^c). (*b*) Experimentally observed attractor. Vertical axis: V_1 (1 V/div); horizontal axis: V_2 (200 mV/div). Positive-going intersections of the trajectory through the plane defined by $I_3 = 1.37$ mA are shown highlighted.

the time domain, a quasi-periodic signal looks like an amplitude-modulated waveform. In state space, a quasi-periodic limit set corresponds to a torus (see figure 2).

(iv) *Chaotic steady-state solution*

Chaos may be defined as *bounded steady-state behaviour in a low-dimensional deterministic dynamical system which is not an equilibrium point, not periodic, and not quasi-periodic* (Parker & Chua 1989).

Attracting equilibrium point, periodic, and quasi-periodic solutions of deterministic dynamical systems have the property that trajectories from nearby initial conditions which converge to the same limit set become correlated with time. By contrast, two trajectories started close together on an attracting *chaotic* limit set diverge expo-

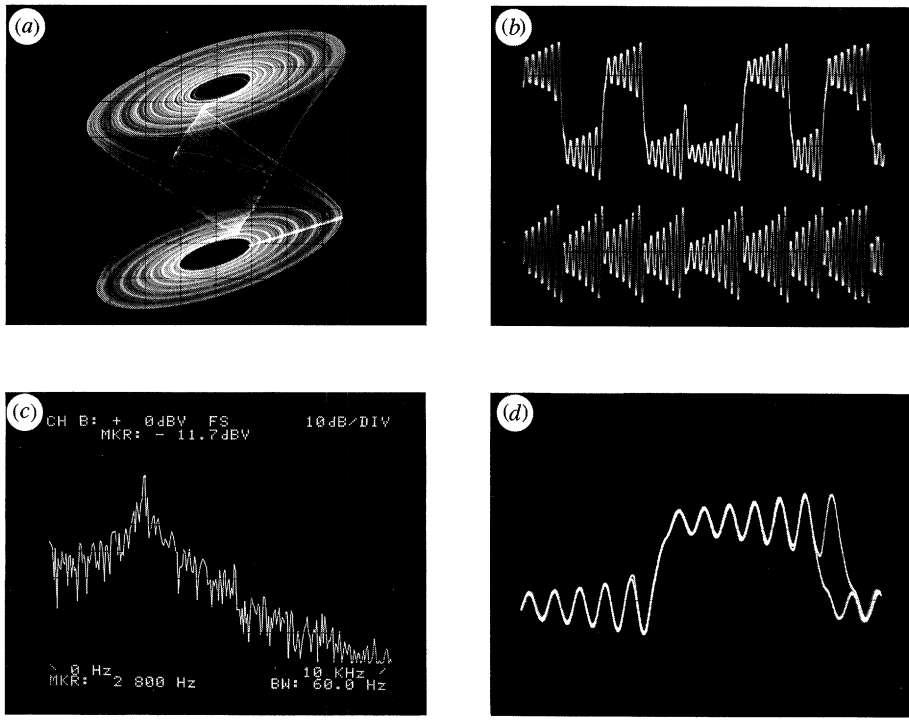

Figure 4. Experimental manifestations of chaos in the double-scroll Chua attractor from Chua's oscillator ($R = 1800\ \Omega$, $C_1 = 9.4$ nF) (see § 4). (*a*) Two-dimensional projection of the attractor in state space; vertical axis: V_1 (1 V/div); horizontal axis: V_2 (200 mV/div). (*b*) Time domain waveforms. Upper trace: $V_1(t)$ (2 V/div); lower trace: $V_2(t)$ (500 mV/div); horizontal axis: t (2 ms/div). (*c*) Power spectrum of $V_2(t)$. Vertical axis: power (dB); horizontal axis: frequency (kHz). (*d*) Time domain waveforms showing sensitivity to initial conditions. Vertical axis: $V_1(t)$ (2 V/div); horizontal axis: t (500 μs/div).

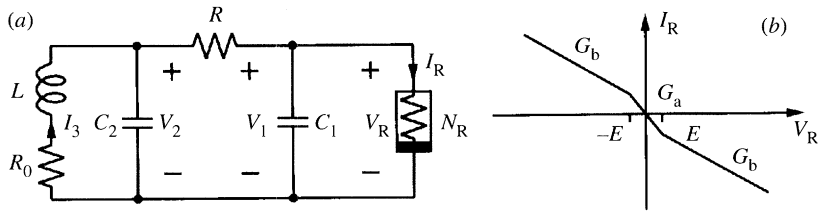

Figure 5. (*a*) Chua's oscillator consists of a linear inductor L with series resistance R_0, a linear resistor R, two linear capacitors C_1 and C_2, and a nonlinear resistor N_R. (*b*) Three-segment piecewise-linear driving-point characteristic of the Chua diode N_R.

nentially and soon become uncorrelated; this is called *sensitive dependence on initial conditions* and gives rise to long-term unpredictability.

How can nearby trajectories diverge exponentially and yet remain within a bounded limit set? This may be achieved by repeated stretching and folding of the flow, as shown in figure 3.

Consider the spiral Chua attractor shown in figure 3. A trajectory spirals away from the equilibrium point P_- along the plane $E^c(P_-)$ until it enters the D_0 region, where it is folded back into D_{-1} and returns to the plane $E^c(P_-)$ close to P_-. The

PHILOSOPHICAL TRANSACTIONS OF THE ROYAL SOCIETY A MATHEMATICAL, PHYSICAL & ENGINEERING SCIENCES

recurrent stretching and folding continues *ad infinitum*, producing a chaotic steady-state solution (Kennedy 1993).

Note that two trajectories passing very close to $\boldsymbol{X}_0$ on $E^{\mathrm{c}}(P_-)$ are separated quite dramatically when they cross the plane U_{-1} and enter D_0. By the time they return to D_{-1}, they are no longer close. This illustrates sensitive dependence on initial conditions.

In the time domain, a chaotic trajectory is neither periodic nor quasi-periodic but looks unpredictable in the long-term. This long-term unpredictability manifests itself in the frequency domain as a broad 'noise-like' power spectrum.

Figure 4*a* shows experimental manifestations of chaos in the well-known double-scroll Chua chaotic attractor from Chua's oscillator (Chua *et al.* 1986).

3. Necessary conditions for chaos in autonomous electronic circuits

We have seen that a dynamical system described by two autonomous first-order ordinary differential equations can have a DC steady-state solution or a periodic steady-state solution. A third state variable is required in order to exhibit more complicated steady-state behaviour.

While a linear circuit can in principle exhibit quasi-periodic motion, the underlying stretching and folding mechanism for generating chaos requires a nonlinearity.

We summarize these observations in the following necessary conditions. In order to exhibit chaos, an autonomous electronic circuit consisting of resistors, capacitors, and inductors must contain at least one locally active resistor, one nonlinear element, and *three* energy-storage elements.

The active resistor supplies energy to separate trajectories, the nonlinearity provides folding, and the three-dimensional state space permits persistent stretching and folding in a bounded region of state space without violating the *non-crossing property* of trajectories.

4. Chua's oscillator

The most widely studied continuous-time autonomous electronic circuit which satisfies the necessary conditions for chaos is Chua's oscillator (this volume). The circuit contains a linear inductor, two linear resistors, two linear capacitors, and a nonlinear resistor N_{R} called a *Chua diode* (Kennedy 1992).

Chua's oscillator is described by three ordinary differential equations:

$$\begin{aligned}
\frac{\mathrm{d}V_1}{\mathrm{d}t} &= \frac{G}{C_1}(V_2 - V_1) - \frac{1}{C_1} f(V_1), \\
\frac{\mathrm{d}V_2}{\mathrm{d}t} &= \frac{G}{C_2}(V_1 - V_2) + \frac{1}{C_2} I_3, \\
\frac{\mathrm{d}I_3}{\mathrm{d}t} &= -\frac{1}{L} V_2 - \frac{R_0}{L} I_3,
\end{aligned}$$

where $G = 1/R$ and $f(V_{\mathrm{R}}) = G_{\mathrm{b}} V_{\mathrm{R}} + \frac{1}{2}(G_{\mathrm{a}} - G_{\mathrm{b}})(|V_{\mathrm{R}} + E| - |V_{\mathrm{R}} - E|)$ is the three-segment piecewise-linear driving-point characteristic of the Chua diode (see figure 5*b*).

This circuit is *canonical* in the sense that every continuous three-dimensional odd-symmetric piecewise-linear vector field may be mapped onto it. The circuit can ex-

hibit *every dynamical behaviour* known to be possible in an autonomous dynamical system described by a continuous odd-symmetric three-region piecewise-linear vector field (Chua, this volume).

In this work, we use Chua's oscillator to illustrate by experiment some aspects of chaos in autonomous electronic circuits. Our practical realization of this circuit is detailed in Appendix A.

The piecewise-linear nature of the nonlinearity in Chua's oscillator divides the state space of the circuit into three distinct affine (linear with an offset) regions, labelled D_{-1} ($V_1 < E$), D_0 ($|V_1| \leqslant E$), and D_1 ($V_1 > E$), separated by boundary planes U_{-1} and U_1 (see figure 3*a*). In each of the affine regions, the circuit has an equilibrium point with saddle-focus stability (Kennedy 1993). Associated with each equilibrium point are two complex eigenvalues with a corresponding eigenplane E^{c}, and a real eigenvalue with associated eigenvector E^{r}.

A trajectory in the D_0 region may be decomposed into its components along the stable complex eigenplane $E^{\mathrm{c}}(0)$ and along the unstable real eigenvector $E^{\mathrm{r}}(0)$. The component along $E^{\mathrm{c}}(0)$ spirals towards the equilibrium point at the origin while the component in the direction $E^{\mathrm{r}}(0)$ grows exponentially away from the origin, so that the trajectory eventually enters one of the outer regions.

A trajectory in the D_{-1} region may be decomposed into its components along the unstable complex eigenplane $E^{\mathrm{c}}(0)$ and along the stable real eigenvector $E^{\mathrm{r}}(0)$. The component on $E^{\mathrm{c}}(P_-)$ spirals away from the equilibrium point P_- along this plane while the component in the direction $E^{\mathrm{r}}(P_-)$ tends asymptotically towards P_-. The strong rate of contraction along the $E^{\mathrm{r}}(P_-)$ direction means that a trajectory spends most of its time in D_{-1} coasting very close to $E^{\mathrm{c}}(P_-)$ (see figure 3). Consequently, the system appears locally to be almost two-dimensional and can therefore be readily analysed using approximate one-dimensional discrete maps, as we shall see in § 5 *e*.

5. Experimental manifestations of chaos

(*a*) *Bifurcations and chaos*

It is often difficult to conclude from experimental data alone whether irregular behaviour observed in an experiment is due to measurement noise or to underlying chaotic dynamics. If, upon adjusting a control parameter, one of the known *routes to chaos* is observed, this indicates that the dynamics might be chaotic.

A *bifurcation* is a qualitative change in the steady-state solution of a system. A *route to chaos* is a continuous path with respect to the parameters of a dynamical system along which the steady-state behaviour of the system changes (through a series of bifurcations) from a stationary or periodic solution to chaos.

The *period-doubling route to chaos* is characterized by an infinite cascade of period-doubling bifurcations as a parameter is increased or decreased. Each period-doubling bifurcation transforms a limit cycle smoothly into one with half the frequency (twice the period), thereby spreading the energy of the system over a wider range of frequencies. An infinite cascade of such doublings results in a chaotic trajectory of infinite period with a broad frequency spectrum which contains energy at all frequencies.

By reducing the variable resistor R in figure 5 from 2000 Ω towards zero, Chua's oscillator exhibits a Hopf-like bifurcation from DC equilibrium, a sequence of period-doubling bifurcations to a spiral Chua chaotic attractor, windows of periodic behaviour, double-scroll Chua chaotic attractors, and a boundary crisis (Kennedy

PHILOSOPHICAL TRANSACTIONS OF THE ROYAL SOCIETY A MATHEMATICAL, PHYSICAL & ENGINEERING SCIENCES

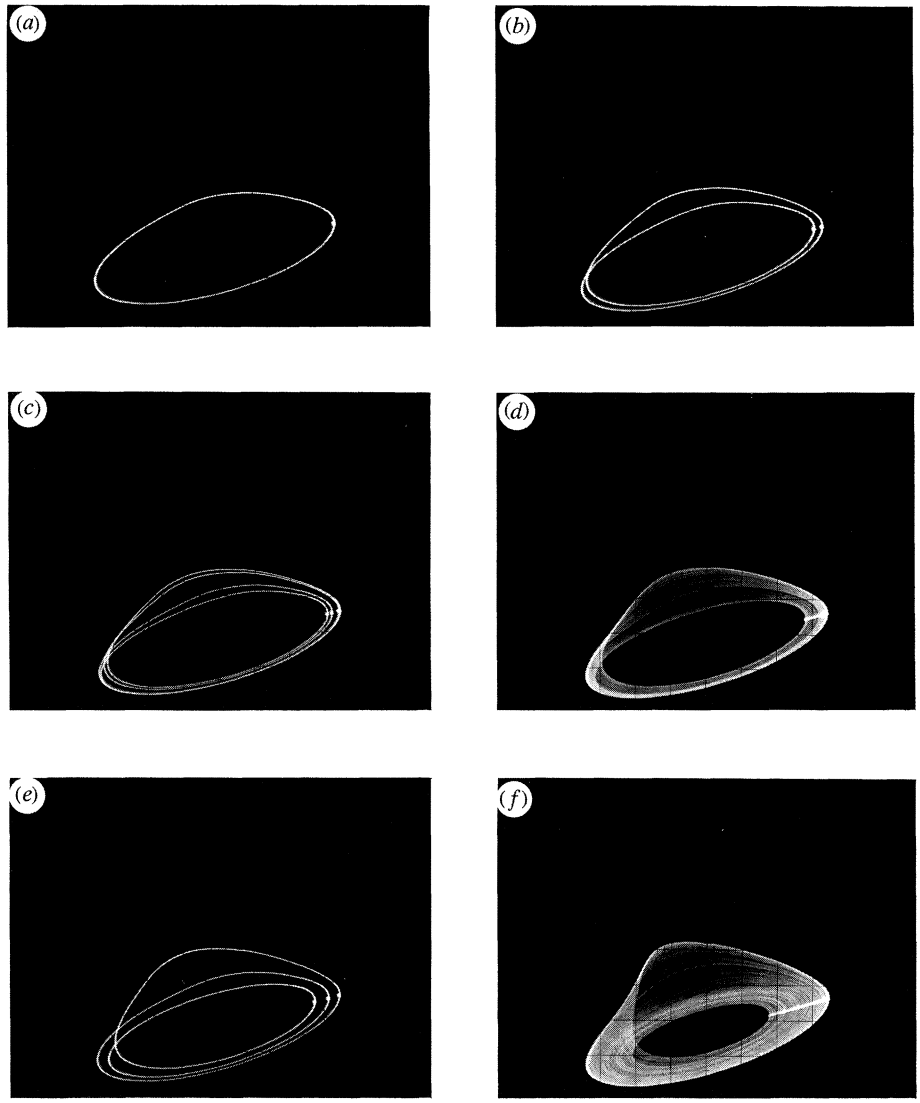

Figure 6. Experimental bifurcation sequence for Chua's oscillator showing the period-doubling route to chaos (*a*)–(*d*), a period-three limit cycle in a periodic window (*e*), and a spiral Chua chaotic attractor (*f*). (*a*) $C_1 = 10.2$ nF (period-one limit cycle); (*b*) $C_1 = 9.8$ nF (period-two limit cycle); (*c*) $C_1 = 9.7$ nF (period-four limit cycle); (*d*) $C_1 = 9.6$ nF (chaotic attractor with Möbius band-like structure); (*e*) $C_1 = 9.55$ nF (period-three limit cycle); (*f*) $C_1 = 9.5$ nF (spiral Chua chaotic attractor). Horizontal axis: $V_2(t)$ (200 mV/div); Vertical axis: $V_1(t)$ (1 V/div). Negative-going intersections of the trajectory through the plane defined by $I_3 = 1.37$ mA are shown highlighted.

1993). An alternative way to view a bifurcation sequence is by adjusting C_1. Fix the value of R at 1800 Ω and vary C_1. To obtain a two-dimensional projection of the three-dimensional state space, plot V_1 versus V_2, for example, using an oscilloscope in X–Y mode. The full range of dynamical behaviours from equilibrium through Hopf, and period-doubling bifurcations, periodic windows, spiral Chua and double-scroll

PHILOSOPHICAL TRANSACTIONS OF THE ROYAL SOCIETY A MATHEMATICAL, PHYSICAL & ENGINEERING SCIENCES

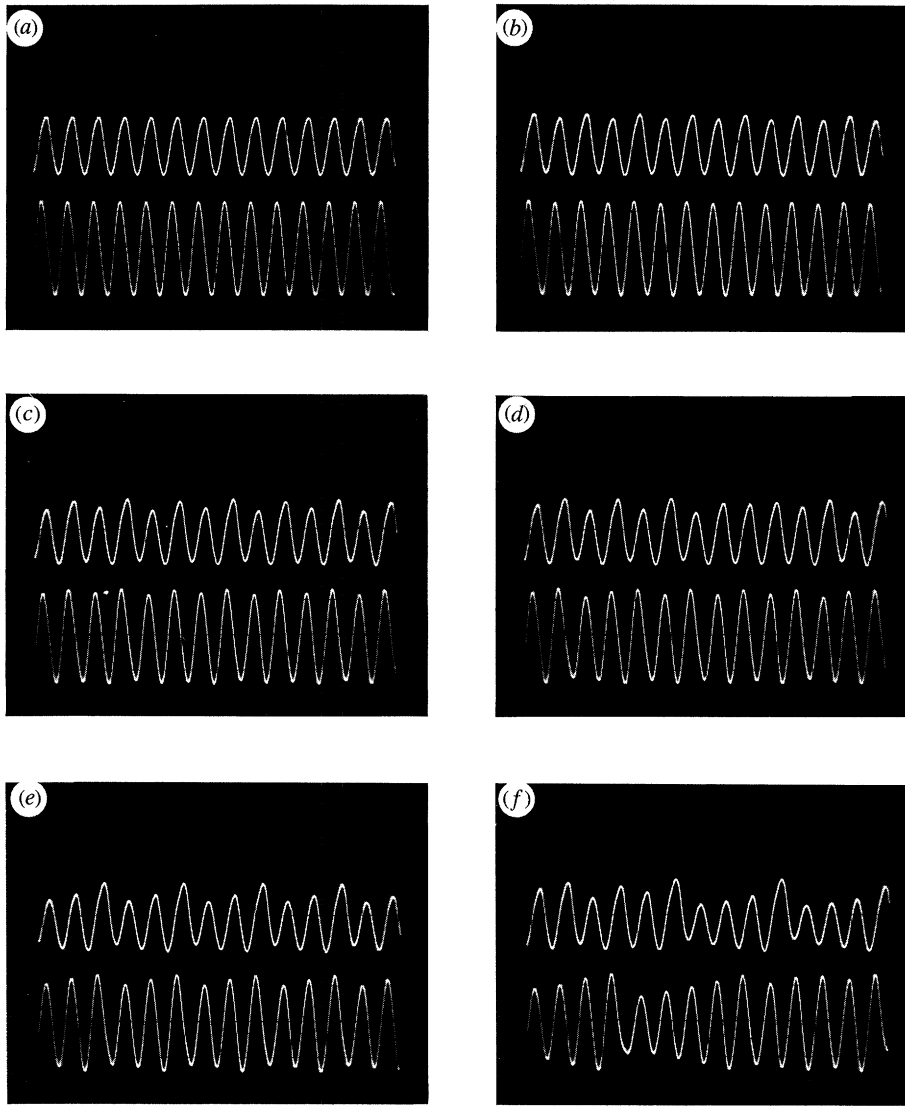

Figure 7. Experimental bifurcation sequence for Chua's oscillator showing period-doubling (*a*)–(*d*), a periodic window (*e*), and spiral Chua chaotic attractor (*f*). Compare with figure 6. (*a*) $C_1 = 10.2$ nF (period-one limit cycle); (*b*) $C_1 = 9.8$ nF (period-two limit cycle); (*c*) $C_1 = 9.7$ nF (period-four limit cycle); (*d*) $C_1 = 9.6$ nF (chaotic attractor with Möbius band-like structure); (*e*) $C_1 = 9.55$ nF (period-three limit cycle); (*f*) $C_1 = 9.5$ nF (spiral Chua chaotic attractor). Upper trace: $V_1(t)$ (2 V/div); Lower trace: $V_2(t)$ (500 mV/div); Horizontal axis: t (500 μs/div).

Chua chaotic attractors can be observed as C_1 is reduced from 11.0 to 7.0 nF (see figures 6 and 4).

(*b*) *Randomness in the time domain*

Figures 7*a*–*f* show the voltage waveforms $V_1(t)$ (upper trace) and $V_2(t)$ (lower trace) corresponding to the attractors shown in figures 6*a*–*f*. The 'period-one' waveform is periodic; it looks like a slightly distorted sinusoid. The 'period-two' waveform

PHILOSOPHICAL TRANSACTIONS OF THE ROYAL SOCIETY A MATHEMATICAL, PHYSICAL & ENGINEERING SCIENCES

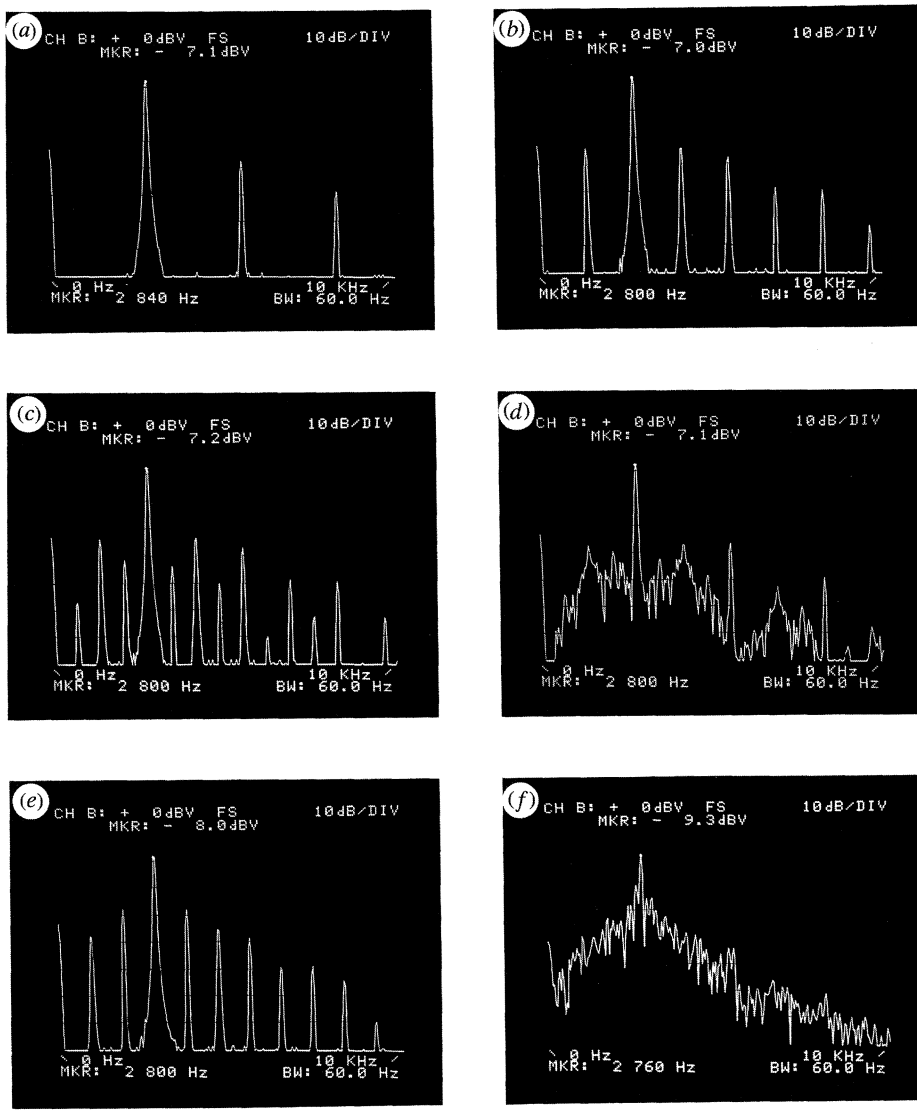

Figure 8. Measured power spectra for attractors in Chua's oscillator using an HP3582A Spectrum Analyzer with Hanning window. Compare with figures 6*a–f* and 7*a–f*. (*a*) Period-one limit cycle, the power spectrum consists of a fundamental frequency and higher harmonics; (*b*) period-two limit cycle, this periodic signal is characterized by a discrete power spectrum; (*c*) period-four limit cycle, the fundamental frequency is roughly one quarter that of (*a*); signal is characterized by a discrete power spectrum; (*d*) chaotic attractor, the chaotic waveform has a broadband power spectrum but still strong periodicity; (*e*) period-three limit cycle, the fundamental frequency is at approximately one third that of (*a*); (*f*) spiral Chua chaotic attractor, broad spectrum with little periodicity evident. Horizontal axis: frequency (kHz); Vertical axis: power (mean squared amplitude of $V_2(t)$) (dB).

is also periodic. It differs qualitatively from 'period-one' in that the pattern of a large peak followed by a small peak repeats approximately once every *two* cycles of the period-one signal; this is why it is called 'period-two.' Similarly, the pattern of large

PHILOSOPHICAL TRANSACTIONS OF THE ROYAL SOCIETY A MATHEMATICAL, PHYSICAL & ENGINEERING SCIENCES

and small peaks in the 'period-four' waveform repeats approximately once every *four* cycles of the period-one signal.

In contrast to these periodic time waveforms, $V_1(t)$ and $V_2(t)$ for the chaotic attractors ((*d*) and (*f*)) are quite irregular and do not appear to repeat themselves in any observation period of finite length. Although they are produced by a third-order *deterministic* dynamical system, the patterns of large and small peaks look 'random.'

(*c*) *Broadband power spectrum*

Every periodic signal may be decomposed into a Fourier series—a weighted sum of sinusoids at integer multiples of a fundamental frequency (Oppenheim *et al.* 1983). Thus, a periodic signal appears in the frequency domain as a set of spikes at the fundamental frequency and its harmonics. The amplitudes of these spikes correspond to the coefficients in the Fourier series expansion. The Fourier transform is an extension of these ideas to aperiodic signals; one considers the distribution of the signal's power over a continuum of frequencies rather than on a discrete set of harmonics (Oppenheim *et al.* 1983).

The distribution of power in a signal $X(t)$ is most commonly quantified by means of the *power density spectrum*, often simply called the *power spectrum*. The simplest estimator of the power spectrum is the periodogram (Oppenheim *et al.* 1983) which, given N uniformly spaced samples $X(m/f_s)$, $m = 0, 1, \ldots, N-1$ of $X(t)$, yields $N/2+1$ numbers $P(nf_s/N)$, $n = 0, 1, \ldots, N/2$, where f_s is the sampling frequency.

If one considers the signal $X(t)$ as being composed of sinusoidal components at discrete frequencies, then $P(nf_s/N)$ is an estimate of the power in the component at frequency nf_s/N. By Parseval's theorem, the sum of the power in each of these components equals the mean squared amplitude of the N samples of $X(t)$ (Oppenheim *et al.* 1983).

If $X(t)$ is *periodic*, then its power will be concentrated in a DC component, a fundamental frequency component, and uniformly spaced harmonics. In practice, the discrete nature of the sampling process causes power to 'leak' between adjacent frequency components; this leakage may be reduced by 'windowing' the measured data before calculating the periodogram (Oppenheim *et al.* 1983).

We remarked earlier that the period-one time waveform corresponding to the attractor in figure 6*b*, is almost sinusoidal; we expect, therefore, that most of its power should be concentrated at the fundamental frequency. The power spectrum of the period-one waveform $V_2(t)$ shown in figure 8*a* consists of a sharp spike at approximately 2.8 kHz and higher harmonic components which are over 30 dB less than the fundamental.

Because the period-two waveform repeats roughly once every 0.7 ms, this periodic signal has a fundamental frequency component at approximately 1.4 kHz (see figure 8*b*). Notice, however, that most of the *power* in the signal is concentrated close to 2.8 kHz. The period-four waveform shown in figure 7*c* has a fundamental frequency of approximately 0.7 kHz (see figure 8*c*).

The spiral Chua chaotic attractor is qualitatively different from these periodic signals. The aperiodic nature of its time-domain waveforms is reflected in the broadband noise-like power spectrum (figure 8*d*). No longer is the power of the signal concentrated in a small number of frequency components; rather, it is distributed over a broad range of frequencies. This broadband structure of the power spectrum persists even if the spectral resolution is increased by sampling at a higher frequency f_s.

PHILOSOPHICAL TRANSACTIONS OF THE ROYAL SOCIETY A MATHEMATICAL, PHYSICAL & ENGINEERING SCIENCES

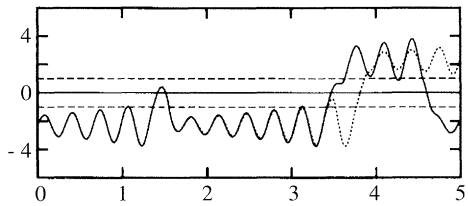

Figure 9. Sensitive dependence on initial conditions. Two simulated time waveforms $V_1(t)$ from Chua's oscillator starting from initial conditions which differ by less that 0.01% in the V_2 coordinate. Note that the trajectories diverge within 5 ms because the solid one crosses to D_1 before the dashed one. Horizontal axis: t (ms); vertical axis: V_1 (V). Compare with figure 4*d*.

The chaotic time waveform due to motion on the double-scroll Chua chaotic attractor also possesses a broad noise-like power spectrum, as shown in figure 4*c*.

(*d*) *Sensitive dependence on initial conditions*

Consider once more the spiral Chua attractor shown in figure 3*a*. A trajectory originating in the lower affine region labelled D_{-1} spirals away from the equilibrium point until it crosses the separating plane U_{-1} and enters the middle region, where it is comes under the influence of the D_0 dynamics. In the case illustrated, the dynamics of the middle region turn the trajectory back into D_{-1}.

In the double-scroll Chua attractor (figure 4), more complicated dynamics are possible. The complex eigenplane $E^{\mathrm{c}}(0)$ separates trajectories entering from an outer region into those which are returned directly to that region and those which transfer across D_0. In this case, two trajectories starting from distinct but almost identical initial states in D_{-1} will remain 'close together' until they reach the separating plane U_{-1} ($V_1 = -E$ in this example). Imagine that the trajectories are still 'close' at the knife-edge presented by $E^{\mathrm{c}}(0)$ at U_{-1}, but that one trajectory crosses into D_0 slightly above $E^{\mathrm{c}}(0)$ and the other slightly below $E^{\mathrm{c}}(0)$. The former trajectory returns to D_{-1}, while the latter crosses over to D_1; their 'closeness' is lost.

The time-domain waveforms $V_1(t)$ for two such trajectories are shown in figure 9*a*. These are solutions of Chua's oscillator with the same parameters as in figure 3; the initial conditions are $(I_3, V_2, V_1) = (1.810\ \mathrm{mA}, 222.014\ \mathrm{mV}, -2.286\ \mathrm{V})$ [solid line] and $(I_3, V_2, V_1) = (1.810\ \mathrm{mA}, 222.000\ \mathrm{mV}, -2.286\ \mathrm{V})$ [dashed line]. Although the initial conditions differ by less than 0.01% in just one component (V_2), the trajectories diverge and become uncorrelated within 5 ms (Kennedy 1993).

Because chaotic systems are *deterministic*, two trajectories which start from *identical* initial states will follow precisely the same paths through the state space. In practice, it is impossible to construct two systems with identical parameters, let alone to start them from identical initial states. However, recent work by Pecora & Carroll (1990) and others has shown that it is possible to *synchronize* two chaotic systems so that their trajectories remain close (Ogorzałek 1993; Hasler 1994). These ideas are now being exploited in secure communication systems where information modulated onto a 'random' chaotic carrier can be demodulated using a synchronized receiver (Dedieu *et al.* 1993; Hasler, this volume).

(*e*) *Poincaré sections and Poincaré maps*

Thus far, we have considered autonomous continuous-time electronic circuits in the time and frequency domains. Further insight into the steady-state behaviour of

PHILOSOPHICAL TRANSACTIONS OF THE ROYAL SOCIETY A MATHEMATICAL, PHYSICAL & ENGINEERING SCIENCES

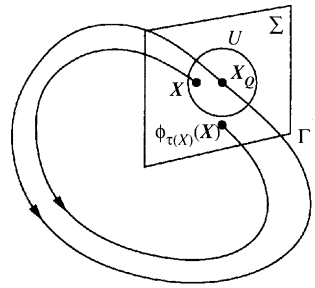

Figure 10. A transverse Poincaré section Σ through the flow of a dynamical system induces a discrete Poincaré map from a neighbourhood U of the point of intersection $\boldsymbol{X_Q}$ to Σ.

a circuit may be gained by means of a geometrical technique due to Poincaré. The idea is to take a cross-section through the limit set in state space and to consider the *discrete-time* dynamical system induced by intersections of trajectories with this section. In this way, a correspondence can be derived between the original continuous-time system and a discrete-time system of lower dimension.

A *Poincaré section* of an n-dimensional autonomous continuous-time dynamical system is an $(n-1)$-dimensional hyperplane Σ in the state space which is intersected *transversally* (nowhere tangentially) by trajectories of the system (Guckenheimer & Holmes 1983).

Let Γ be a closed trajectory of the flow of a continuous vector field $\boldsymbol{F}$, and let $\boldsymbol{X_Q}$ be a point of intersection of Γ with Σ. If T is the period of Γ and $\boldsymbol{X} \in \Sigma$ is sufficiently close to $\boldsymbol{X_Q}$, then the trajectory $\boldsymbol{\phi}_t(\boldsymbol{X})$ through $\boldsymbol{X}$ will return to Σ after a time $\tau(\boldsymbol{X}) \approx T$ and intersect the hyperplane at a point $\boldsymbol{\phi}_{\tau(\boldsymbol{X})}(\boldsymbol{X})$, as shown in figure 10.

This construction implicitly defines a function (called a *Poincaré map* or *first return map*) $\boldsymbol{G} : U \to \Sigma$

$$\boldsymbol{G}(\boldsymbol{X}) = \boldsymbol{\phi}_{\tau(\boldsymbol{X})}(\boldsymbol{X}),$$

where U is a small region of Σ close to $\boldsymbol{X_Q}$.

If trajectories of the continuous-time dynamical system are non-crossing, there is a one-to-one correspondence between a trajectory of (2.1) and a sequence of iterates of the discrete-time system,

$$\boldsymbol{X}_{k+1} = \boldsymbol{G}(\boldsymbol{X}_k), \tag{5.1}$$

defined by the Poincaré map. Indeed, $\boldsymbol{X}_k \equiv \boldsymbol{\phi}_{t_k}(\boldsymbol{X}_0)$, where $\{t_k, k \in \mathbb{N}\}$ are the times of intersection of $\boldsymbol{\phi}_t(\boldsymbol{X}_0)$ with Σ.

In the case of a three-dimensional autonomous continuous-time system, the cutting plane Σ is two-dimensional. For example, in Chua's oscillator, we can define a cutting plane by $I_3 = I_\Sigma$. The flow of the circuit takes a point $(V_1(t_k), V_2(t_k), I_\Sigma)$ to the point $(V_1(t_{k+1}), V_2(t_{k+1}), I_\Sigma)$. Thus, we have a two-dimensional Poincaré map from $(V_1(t_k), V_2(t_k)) \in \Sigma$ to $(V_1(t_{k+1}), V_2(t_{k+1}) \in \Sigma$.

Since the construction of the Poincaré map preserves the one-to-one relationship between the three-dimensional flow and the two-dimensional discrete map, the map itself cannot be one-dimensional. However, because of very strong dissipation in the circuit (for this set of parameters) in the direction of $E^r(P_-)$, the Poincaré section is *almost* one-dimensional. In fact, repeated stretching and folding of the flow produces a multi-layered *fractal* structure (Kennedy 1994*b*) with dimension only slightly

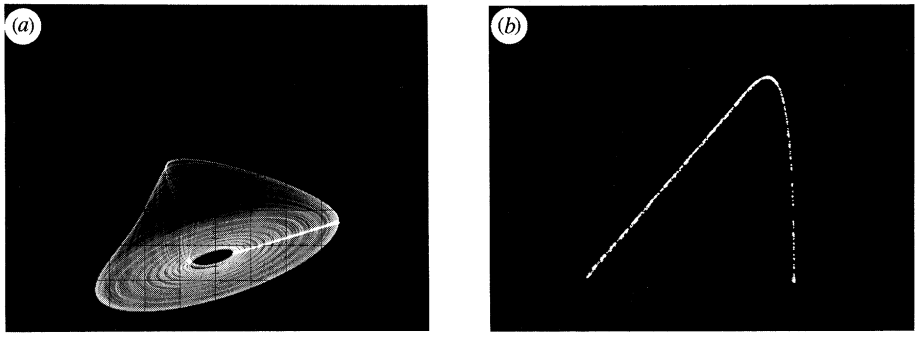

Figure 11. (a) Experimental Poincaré section for Chua's oscillator. Horizontal axis: $V_2(t)$ (200 mV/div); vertical axis: $V_1(t)$ (1 V/div). The points of intersection of the trajectory as I_3 decreases through $I_\Sigma \approx 1.37$ mA are highlighted. (b) Approximate one-dimensional map derived from (a). Horizontal axis: $V_2(t_k)$ (1 V/div); vertical axis: $V_2(t_{k+1})$ (1 V/div).

greater that unity. Thus, we can form an *approximate* one-dimensional Poincaré map from $V_2(t_k)$ to $V_2(t_{k+1})$. We can visualize the underlying shape of this map by plotting successive iterates of $V_2(t_{k+1})$ versus $V_2(t_k)$, as shown in figure 11b.

The stretching and folding mechanism for chaos generation in this system can be inferred by comparing figures 11a and 3a. Figure 11a shows highlighted negative-going intersections of the trajectory $\boldsymbol{\phi}_t(\boldsymbol{X}_0)$ with $I_3 = I_\Sigma$, while figure 3a shows the points of intersection of the trajectory when I_3 increases through I_Σ. The bundle of trajectories in figure 11a (which looks like a line segment) is stretched apart by the flow, folded over on itself like a horseshoe (figure 3b), and flattened once more onto the plane $E^{\mathrm{c}}(P_-)$. Recurrent stretching and folding of the flow in this way produces chaos.

For small values of $V_2(t_k)$, the trajectory lies close to the plane $E^{\mathrm{c}}(P_-)$, where it follows a logarithmic spiral about P_-. This manifests itself in the approximate one-dimensional map as an almost linear region with slope greater than unity. Beyond the value of $V_2(t_k)$ which corresponds to the position of the fold in the cross-section (figure 3b), the trajectory is reinjected from D_0 into D_{-1} progressively closer to P_- as $V_2(t_k)$ increases. The resulting approximate one-dimensional map has a characteristic *unimodal* or *one-hump* shape.

Note that the approximate one-dimensional map is not invertible: two different values of $V_2(t_k)$ can yield the same value of $V_2(t_{k+1})$. It is no coincidence that the underlying one-dimensional map is non-invertible when the attractor is chaotic. Indeed, a discrete-time system described by an *invertible* one-dimensional map cannot exhibit chaos (Ott 1993).

A consequence of Sharkovsky's theorem (Sharkovsky 1964) is that if G is a unimodal map and $X_{k+1} = G(X_k)$ has a period-three orbit, then it has an orbit of every period (Collet & Eckmann 1980). Thus, if the approximate one-dimensional Poincaré map has a period-three orbit (see figure 12e) then it also possesses orbits of all other periods (although none of these may be attracting) (Li & Yorke 1975). This fact can be exploited to produce periodic behaviour of arbitrary period by stabilizing the appropriate unstable periodic orbit (Ott *et al.* 1990; Ogorzałek 1994, 1995).

PHILOSOPHICAL TRANSACTIONS OF THE ROYAL SOCIETY A MATHEMATICAL, PHYSICAL & ENGINEERING SCIENCES

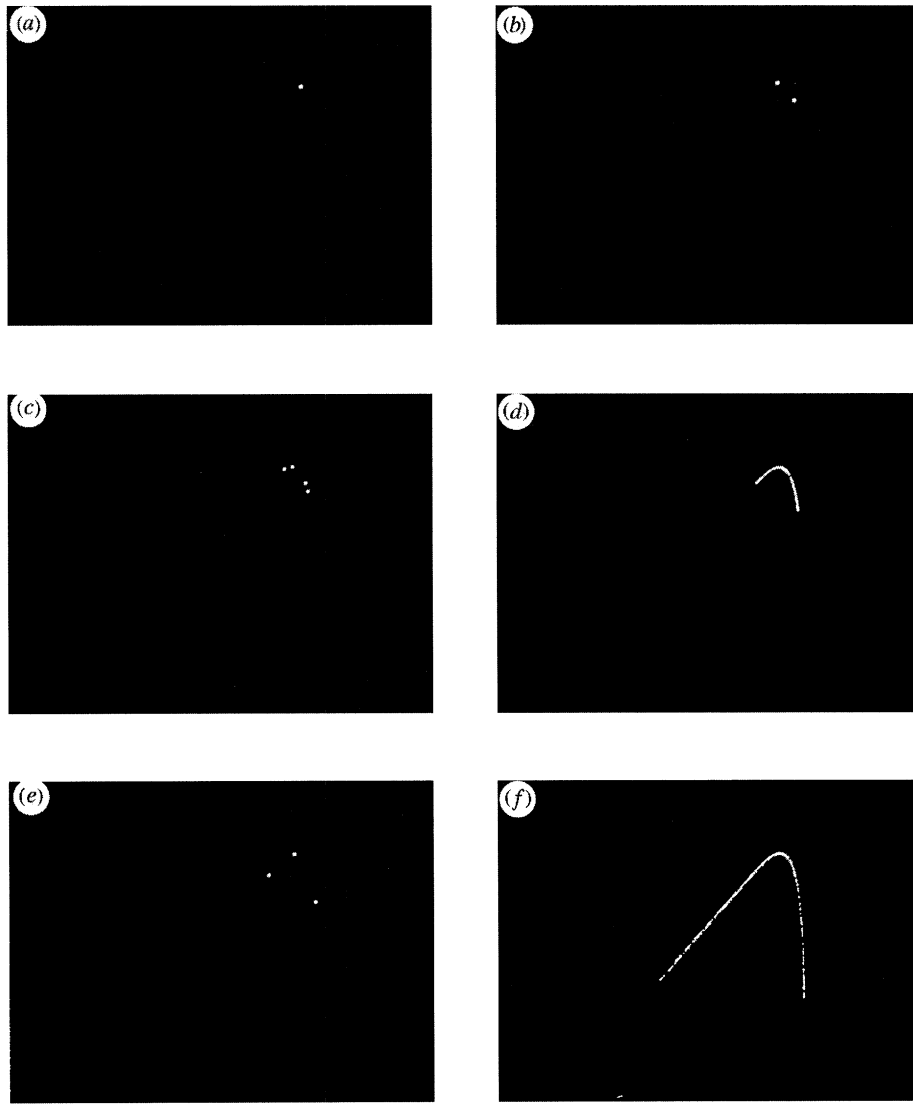

Figure 12. Experimental approximate one-dimensional maps for $V_2(t)$ from Chua's oscillator. Compare with figure 6*a–f*. (*a*) A period-one limit cycle appears as a fixed point of the approximate Poincaré map, $V_{2k+1} = V_{2k}$; (*b*) period-two limit cycle, $V_{2k+2} = V_{2k}$; (*c*) period-four limit cycle, $V_{2k+4} = V_{2k}$; (*d*) chaotic attractor with Möbius band-like structure, steady-state iterates of the approximate one-dimensional map lie on a unimodal curve; (*e*) period-three limit cycle, $V_{2k+3} = V_{2k}$; (*f*) spiral Chua chaotic attractor, iterates of the approximate one-dimensional map suggest the underlying unimodal shape. Horizontal axis: $V_2(t_k)$ (1 V/div); vertical axis: $V_2(t_{k+1})$ (1 V/div).

6. Concluding remarks

In this work, we have discussed the nature of chaotic steady-state behaviour and have described how it manifests itself in autonomous electronic circuits. In our discussions of state space, time- and frequency-domain measurement techniques for characterizing steady-state behaviour, we have concentrated exclusively on the Chua's

PHILOSOPHICAL TRANSACTIONS OF THE ROYAL SOCIETY A MATHEMATICAL, PHYSICAL & ENGINEERING SCIENCES

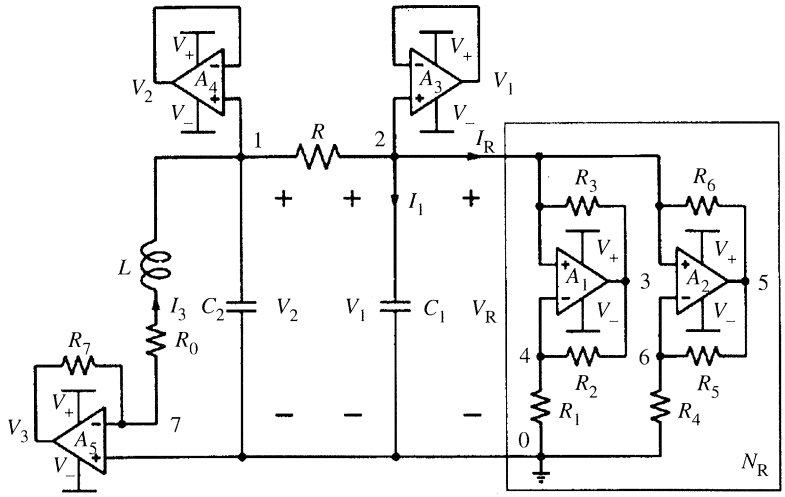

Figure 13. Practical implementation of Chua's circuit using two op amps and six resistors to realize the Chua diode (Kennedy 1992). Component values are listed in table 1. $R_0 = 12.5\ \Omega$ is the parasitic DC series resistance of the TOKO inductor.

circuit paradigm (Madan 1993). Experimental chaos has of course been reported in many autonomous electronic circuits other than those introduced by Chua. Circuits known to exhibit chaos include the continuous-time systems studied by Arnéodo *et al.* (1984), Dmitriev & Kislov (1984), Freire *et al.* (1984), Ogorzałek (1989), Nishio *et al.* (1990), and Kennedy (1994*b*), the hysteretic chaotic circuits studied by Newcomb (1983) and Saito (1985, this volume), and the discrete-time circuits developed by Rodriguez-Vazquez *et al.* (1987).

Appendix A. Practical realization of Chua's oscillator

Figure 13 shows a practical implementation of Chua's oscillator using a dual op amp and six resistors to implement the Chua diode N_R (Kennedy 1992).

The op amp sub-circuit consisting of A_1, A_2 and R_1–R_6 functions as a nonlinear resistor N_R with driving-point characteristic as shown in figure 5*b*. Using two 9 V batteries to power the op amps gives $V^+ = 9$ V and $V^- = -9$ V. From measurements of the saturation levels of the AD712 outputs, $E_{\rm sat} \approx 8.3$ V, giving $E \approx 1$ V. With $R_2 = R_3$ and $R_5 = R_6$, the nonlinear characteristic is defined by $G_{\rm a} = -1/R_1 - 1/R_4 = -50/66$ mS, $G_{\rm b} = 1/R_3 - 1/R_4 = -9/22$ mS, and $E = R_1 E_{\rm sat}/(R_1 + R_2) \approx 1$ V (Kennedy 1992).

Op amps A_3 and A_4 are connected as optional unity-gain buffers. Their outputs are V_1 and V_2, respectively. Op amp A_5 and resistor R_7 together constitute a current-to-voltage converter: $V_3 = I_3 R_7$. If it is not required to measure I_3, node 7 should be shorted to node 0.

Appendix B. Electronic realization of a variable capacitor

A variable capacitor may be implemented by using the op amp circuit shown in figure 14. Op amp A_6 is configured as a unity-gain buffer. It applies a voltage of

Table 1. *Component list for Chua's oscillator with buffered outputs shown in figure 13*

element	description	value	tolerance
A_1	op amp (1/2 AD712, TL082, or equivalent)		
A_2	op amp (1/2 AD712, TL082, or equivalent)		
A_3	op amp (1/4 AD713, TL084, or equivalent)		
A_4	op amp (1/4 AD713, TL084, or equivalent)		
A_5	op amp (1/4 AD713, TL084, or equivalent)		
C_1	capacitor	10 nF	±5%
C_2	capacitor	100 nF	±5%
R	multi-turn potentiometer	2 kΩ	
R_1	1/4 W resistor	3.3 kΩ	±5%
R_2	1/4 W resistor	22 kΩ	±5%
R_3	1/4 W resistor	22 kΩ	±5%
R_4	1/4 W resistor	2.2 kΩ	±5%
R_5	1/4 W resistor	220 Ω	±5%
R_6	1/4 W resistor	220 Ω	±5%
R_7	1/4 W resistor	1 kΩ	±5%
L	inductor (TOKO type 10RB or equivalent)	18 mH	± 10%

$V_1 R_9/(R_8 + R_9)$ to the bottom end of capacitor C_3. If R_8 and R_9 are sufficiently large, then the current into the capacitor is given by

$$I_1 \approx C_3 \left(\frac{R_8}{R_8 + R_9} \right) \frac{\mathrm{d}V_1}{\mathrm{d}t},$$

and the effective capacitance between the terminals is $C_3 R_8/(R_8 + R_9)$.

If C_3 is fixed, and R_8 and R_9 are the resistances above and below the tap on a potentiometer, then the effective capacitance can be varied between 0 and C_3 by moving the position of the tap. The potentiometer must be chosen so that it has negligible loading effect on the rest of the circuit. For the set of parameters used in this paper, suitable choices for C_3 and $(R_8 + R_9)$ are 15 nF and 500 kΩ, respectively.

Appendix C. Poincaré section and approximate one-dimensional map

Figure 15 shows the circuitry used to generate the Poincaré sections and approximate one-dimensional maps shown in figures 6 and 12.

The cutting plane Σ is defined by the reference voltage V_Σ, and may be moved by adjusting the position of the tap on potentiometer R_{10}. The logic output of the comparator CMP is toggled when the selected input $V_i(t)$ crosses through the chosen reference level. If switch S_2 is open, the exclusive-OR gate converts negative-going

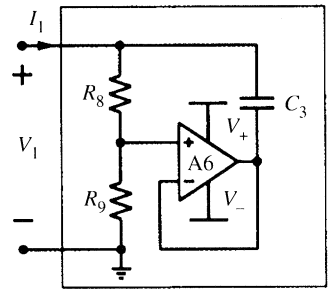

Figure 14. Practical implementation of variable capacitor for Chua's oscillator.

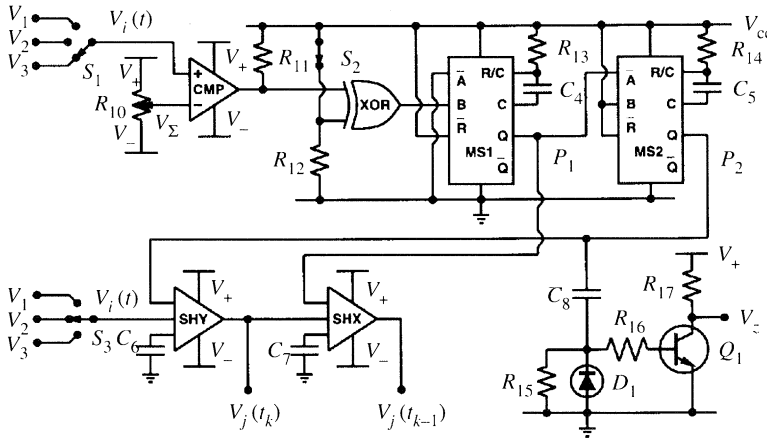

Figure 15. Circuitry to highlight a Poincaré section in Chua's oscillator and to display the corresponding approximate one-dimensional map. Component values are listed in table 2.

transitions of $V_i(t)$ through V_Σ into positive-going edges. If S_2 is closed, a negative-going input produces a positive-going edge at the output of this gate.

A positive-going edge from the output of the exclusive-OR gate triggers monostable MS1 at time t_k. The time-constant of MS1 is chosen so that it produces a 'high' pulse P_1 of width $\delta t \approx 4\,\mu$s. The falling edge of this pulse triggers the second monostable (MS2), which produces a non-overlapping 'high' pulse P_2 also of width δt.

An approximate one-dimensional map may be obtained by selecting $V_j(t)$ with switch S_3. At time t_k, timing pulse P_1 clocks the previously stored sample $V_j(t_{k-1})$ of $V_j(t)$ into sample-and-hold circuit SHX. Pulse P_2 then performs two functions. It provides a blanking signal V_Z for the Z-modulation input of an oscilloscope (via the inverter Q_1) to highlight the point $\boldsymbol{X}(t_k) \in \Sigma$. It simultaneously clocks the new sample $V_j(t_k)$ into sample-and-hold SHY.

The approximate one-dimensional map of V_j may be viewed by connecting the outputs of SHX and SHY to the X- and Y-inputs, respectively, of an oscilloscope in X–Y mode.

A complete list of components is given in table 2. The analogue power rails (V_- and V_+) are ± 9 V; the logic supply V_{CC} is 5 V. We recommend that bypass capacitors of at least 0.1 µF each should be connected between the power supplies and ground, as close to each of the integrated circuits as possible.

Table 2. *Component list for Poincaré section and approximate one-dimensional map circuitry*

element	description	value	tolerance
CMP	comparator (LM311)		
XOR	exclusive-OR gate (1/4 74HC86 or equivalent)		
MS1	monostable (1/2 74HCT123 or equivalent)		
MS2	monostable (1/2 74HCT123 or equivalent)		
SHY	sample and hold (LF398)		
SHX	sample and hold (LF398)		
C_4	capacitor	10 nF	±10%
C_5	capacitor	10 nF	±10%
C_6	capacitor (polystyrene)	1 nF	±10%
C_7	capacitor (polystyrene)	1 nF	±10%
C_8	capacitor	1 nF	±10%
R_{10}	multi-turn potentiometer	10 kΩ	
R_{11}	1/4 W resistor	1 kΩ	±5%
R_{12}	1/4 W resistor	10 kΩ	±5%
R_{13}	1/4 W resistor	1 kΩ	±5%
R_{14}	1/4 W resistor	1 kΩ	±5%
R_{15}	1/4 W resistor	51 Ω	±5%
R_{16}	1/4 W resistor	10 kΩ	±5%
R_{17}	1/4 W resistor	1 kΩ	±5%
D_1	diode (1N4148 or equivalent)		
Q_1	NPN transistor (2N2222 or equivalent)		

References

Arnéodo, A., Coullet, P. & Tresser, C. 1981 Possible new strange attractors with spiral structure. *Commun. Math. Phys.* **79**, 573–579.

Chua, L. O., Desoer, C. A. & Kuh, E. S. 1987 *Linear and nonlinear circuits*. New York: McGraw-Hill.

Chua, L. O., Komuro, M. & Matsumoto, T. 1986 The double scroll family. I, II. *IEEE Trans. Circuits Syst.* **CAS-33**, 1073—1118.

Collet, P. & Eckmann, J.-P. 1980 *Iterated maps on the interval as dynamical systems*. Boston: Birkhäuser.

Dedieu, H., Kennedy, M. P. & Hasler, M. 1993 Chaos shift keying: modulation and demodulation of a chaotic carrier using self-synchronizing Chua's circuits. *IEEE Trans. Circuits Syst.* **CAS-40**, 634–642.

Dmitriev, A. S. & Kislov, V. Y. 1984 Stochastic oscillations in self-excited oscillator with a first-order inertial delay. *Radiotekhnika electronika* **29**, 2389. (In Russian.)

Freire, E., Franquelo, L. G. & Arancil, J. 1984 Periodicity and chaos in an autonomous electronic circuit. *IEEE Trans. Circuits Syst.* **31**, 237–247.

Guckenheimer, J. & Holmes, P. *Nonlinear oscillations, dynamical systems, and bifurcations of vector fields.* New York: Springer.

Hasler, M. 1994 Synchronization principles and applications. In *Circuits and systems tutorials* (ed. C. Toumazou), ch. 6.2, pp. 314–327. IEEE ISCAS'94, London, UK.

Kennedy, M. P. 1992 Robust op amp realization of Chua's circuit. *Frequenz* **46**(3–4).

Kennedy, M. P. 1993 Three steps to chaos. II. A Chua's circuit primer. *IEEE Trans. Circuits Syst.* (Part I) **40**.

Kennedy, M. P. 1994*a* Chaos in the Colpitts oscillator. *IEEE Trans. Circuits Syst.* (Part I) **41**, 771–774.

Kennedy, M. P. 1994*b* Basic concepts of nonlinear dynamics and chaos. In *Circuits and systems tutorials* (ed. C. Toumazou), ch. 6.1, pp. 289–313. IEEE ISCAS'94, London, UK.

Kennedy, M. P. & Chua, L. O. 1986 Van der Pol and chaos. *IEEE Trans. Circuits Syst.* **33**, 974–980.

Li, T. Y. & Yorke, J. A. 1975 Period three implies chaos. *Am. Math. Mon.* **82**, 985–992.

Linsay, P. 1981 Period doubling and chaotic behavior in a driven anharmonic oscillator. *Phys. Rev. Lett.* **47**, 1349–1392.

Madan, R. N. (ed.) 1993 *Chua's circuit: a paradigm for chaos.* Singapore: World Scientific.

Newcomb, R. W. & Sathyan, S. 1983 An RC op amp chaos generator. *IEEE Trans. Circuits Syst.* **30**, 54–56.

Nishio, Y., Inaba, N. & Mori, S. 1990 Chaotic phenomena in an autonomous circuit with nonlinear inductor. *Proc. ISCAS.*

Ogorzałek, M. J. 1989 Order and chaos in a third order RC ladder network with nonlinear feedback. *IEEE Trans. Circuits Syst.* **36**, 1221–1230.

Ogorzałek, M. J. 1993 Taming chaos. I. Synchronisation. *IEEE Trans. Circuits Syst.* **CAS-40**.

Ogorzałek, M. J. 1994 Control concepts and applications. In *Circuits systems tutorials* (ed. C. Toumazou), ch. 6.3, pp. 328–340. IEEE ISCAS'94, London, UK.

Ott, E. 1993 *Chaos in dynamical systems.* Cambridge University Press.

Ott, E., Grebogi, C. & Yorke, J. 1990 Controlling chaos. *Phys. Rev. Lett.* **64**, 1196–1199.

Oppenheim, A. V., Willsky, A. S. & Young, I. T. 1983 *Signals and systems.* Englewood Cliffs, NJ: Prentice-Hall.

Parker, T. S. & Chua, L. O. 1989 *Practical numerical algorithms for chaotic systems.* New York: Springer.

Pecora, L. M. & Carroll, T. L. 1990 Synchronization in chaotic systems. *Phys. Rev. Lett.* **64**, 821—824.

Rodriguez-Vazquez, A., Huertas, J. L., Rueda, A., Perez-Verdu, B. & Chua, L. O. 1987 Chaos from switched-capacitor circuits: discrete maps. *Proc. IEEE* **75**, 1090–1106.

Ruelle, D. & Takens, F. 1971 On the nature of turbulence. *Commun. Math. Phys.* **20**, 167–192.

Saito, T. 1985 On a hysteresis chaos generator. In *Proc. ISCAS '85*, pp. 847–849. Kyoto: Japan.

Sharkovsky, A. N. 1964 Coexistence of cycles of a continuous map of the line into itself. *Ukr. Mat. Z.* **16**, 61–71.

Testa, J., Pérez, J. & Jeffries, C. 1982 Evidence for universal chaotic behavior of a driven nonlinear oscillator. *Phys. Rev. Lett.* **48**, 714–717.

Thompson, J. M. T. & Stewart, H. B. 1986 *Nonlinear dynamics and chaos.* New York: Wiley.

Ueda, Y. & Akamatsu, N. 1980 Chaotically transitional phenomena in the forced negative-resistance oscillator. *IEEE Trans. Circuits Syst.* **CAS-28**, 217–224.

van der Pol, B. & vander Mark, J. 1927 Frequency demultiplication. *Nature* **120**, 363–364.

Vidyasagar, M. *Nonlinear systems analysis.* Englewood Cliffs, NJ: Prentice-Hall.

PHILOSOPHICAL TRANSACTIONS OF THE ROYAL SOCIETY A MATHEMATICAL, PHYSICAL & ENGINEERING SCIENCES

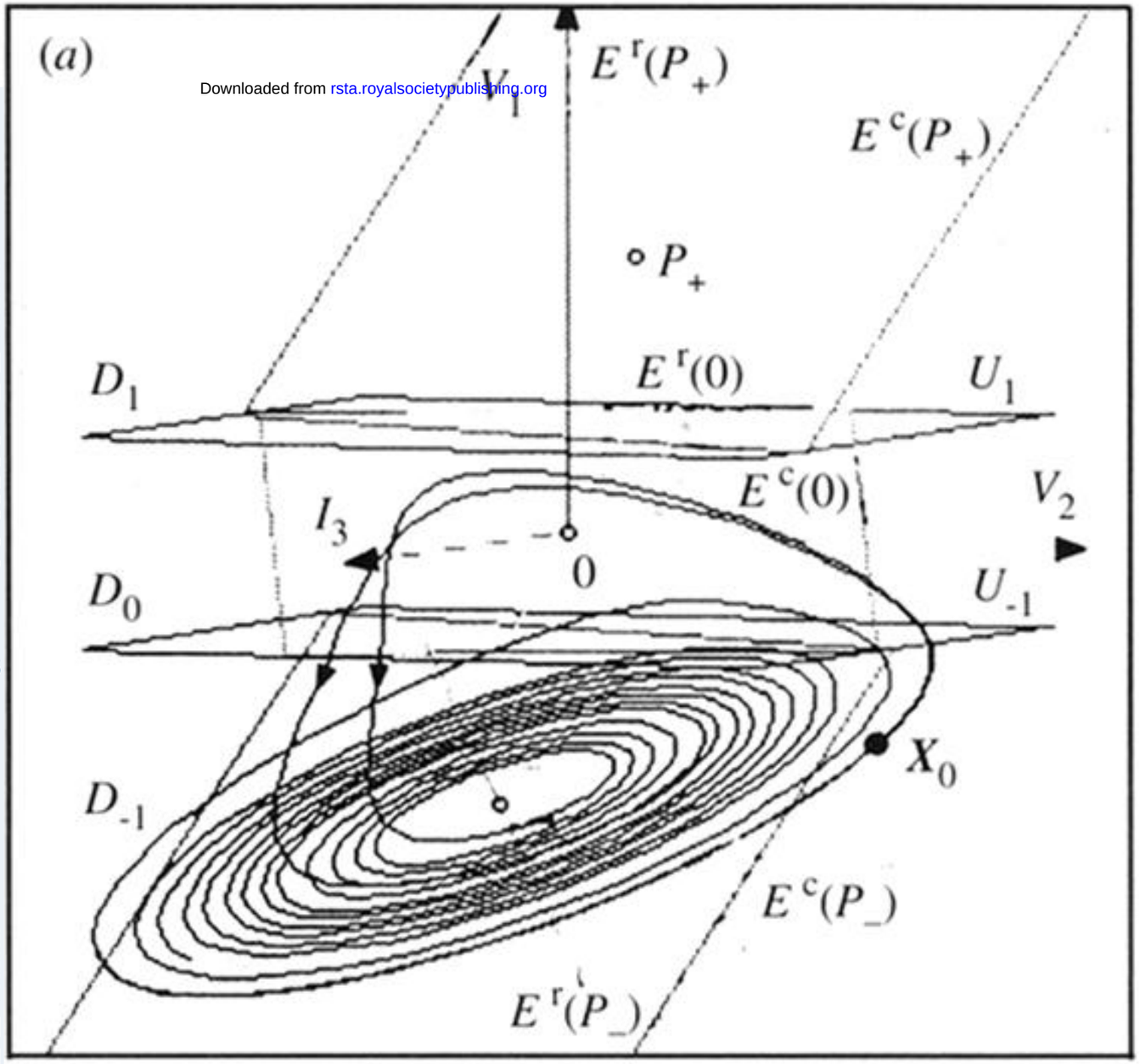

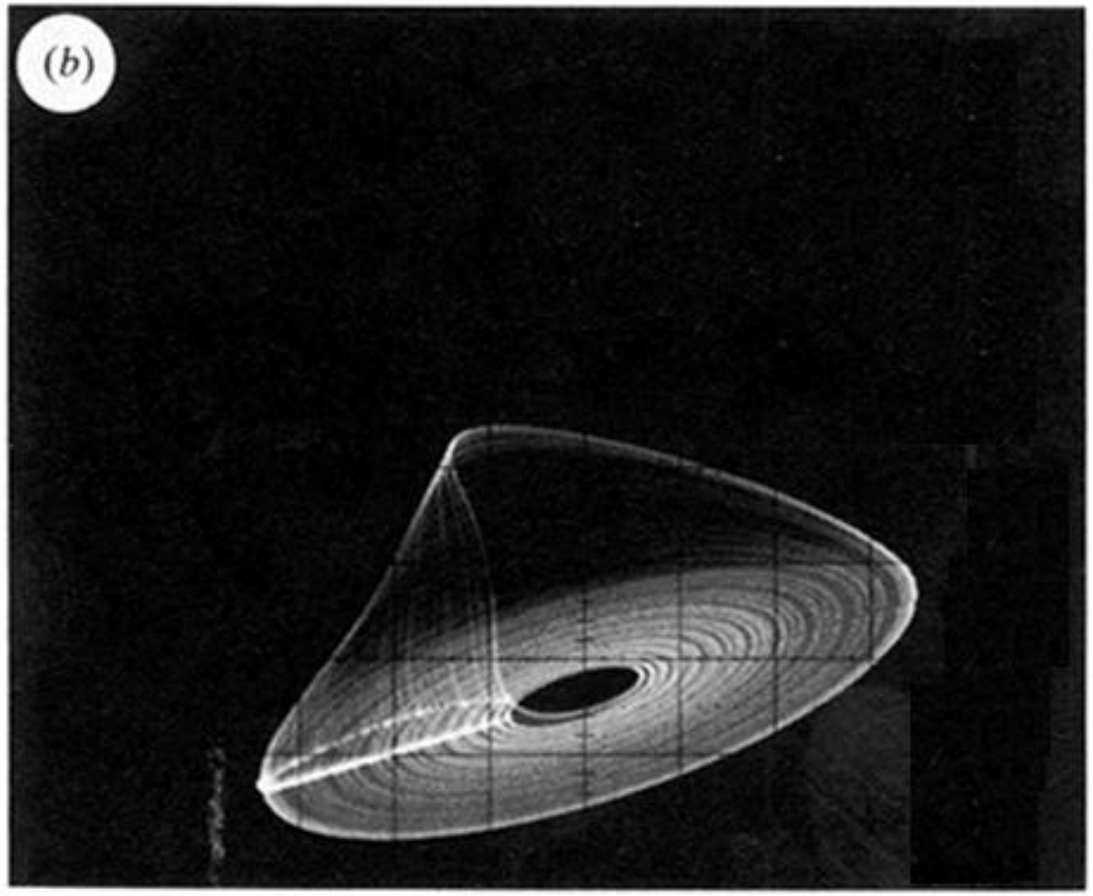

Figure 3. Stretching and folding mechanism of chaos generation in Chua's oscillator (see § 4). (*a*) Simulated spiral Chua chaotic attractor showing affine regions (D_{-1} and D_1), separating planes (U_{-1} and U_1), equilibrium points (P_-, 0, and P_+), and their associated eigenspaces (E^r and E^c). (*b*) Experimentally observed attractor. Vertical axis: V_1 (1 V/div); horizontal axis: V_2 (200 mV/div). Positive-going intersections of the trajectory through the plane defined by $I_3 = 1.37$ mA are shown highlighted.

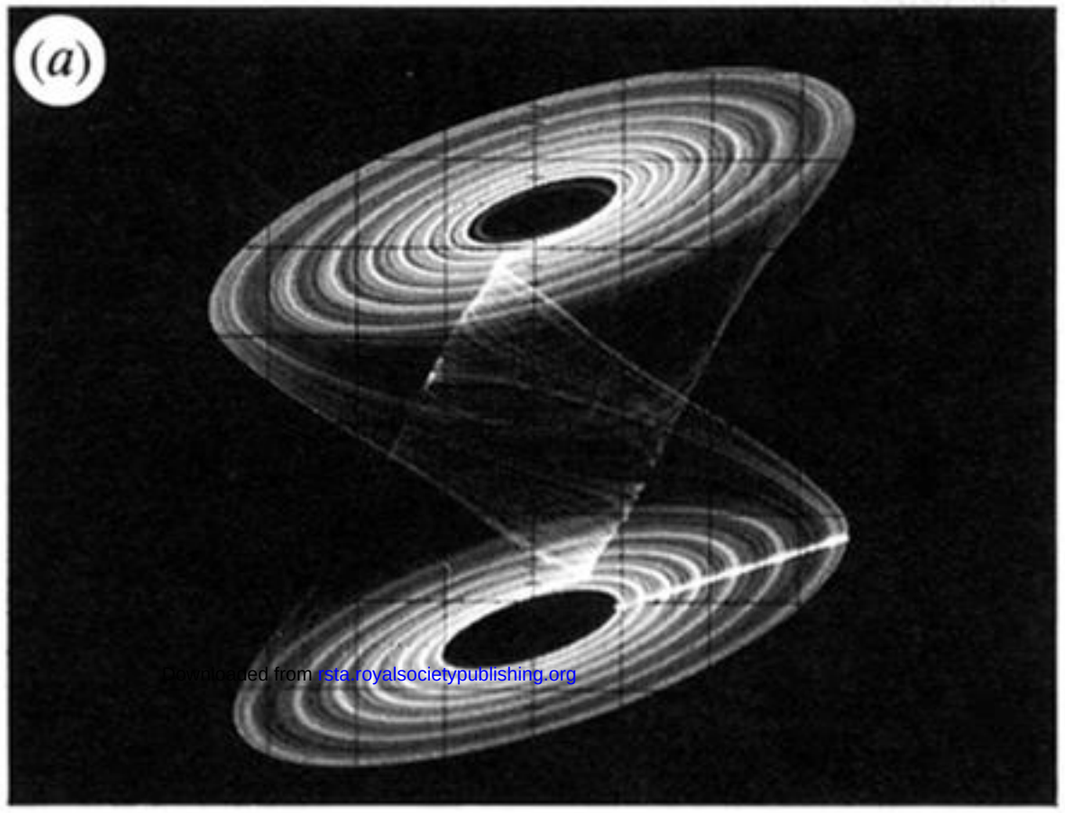

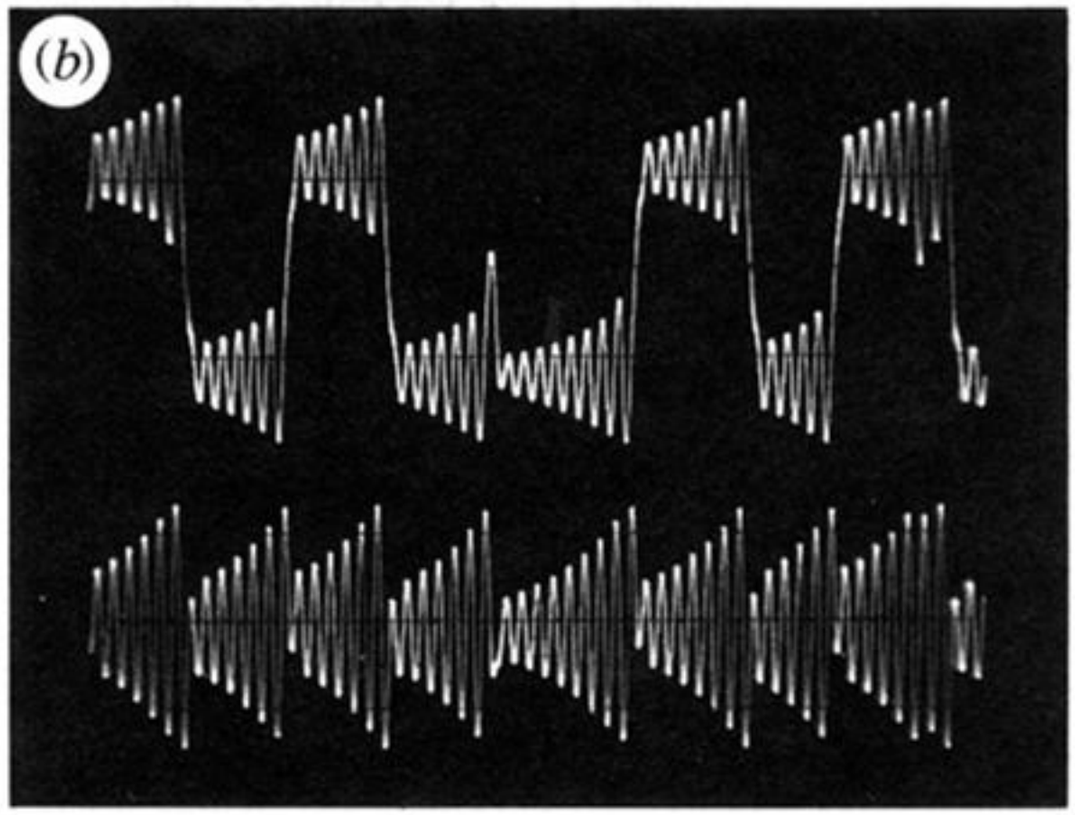

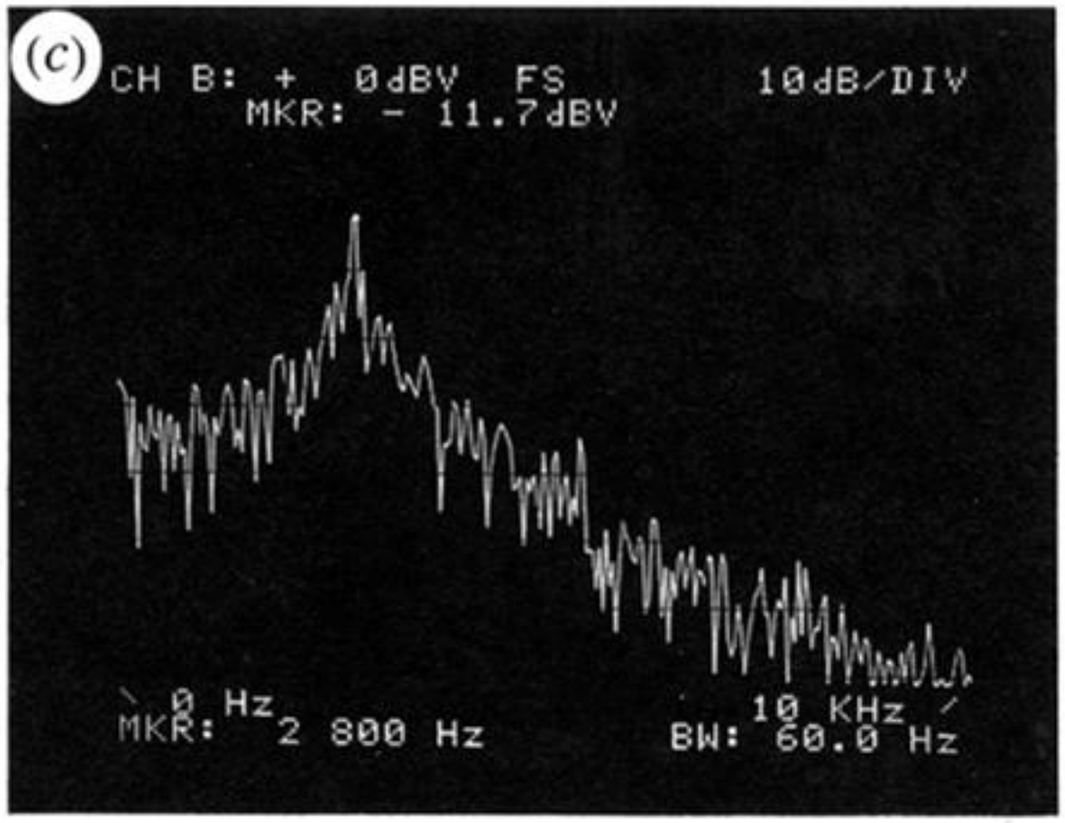

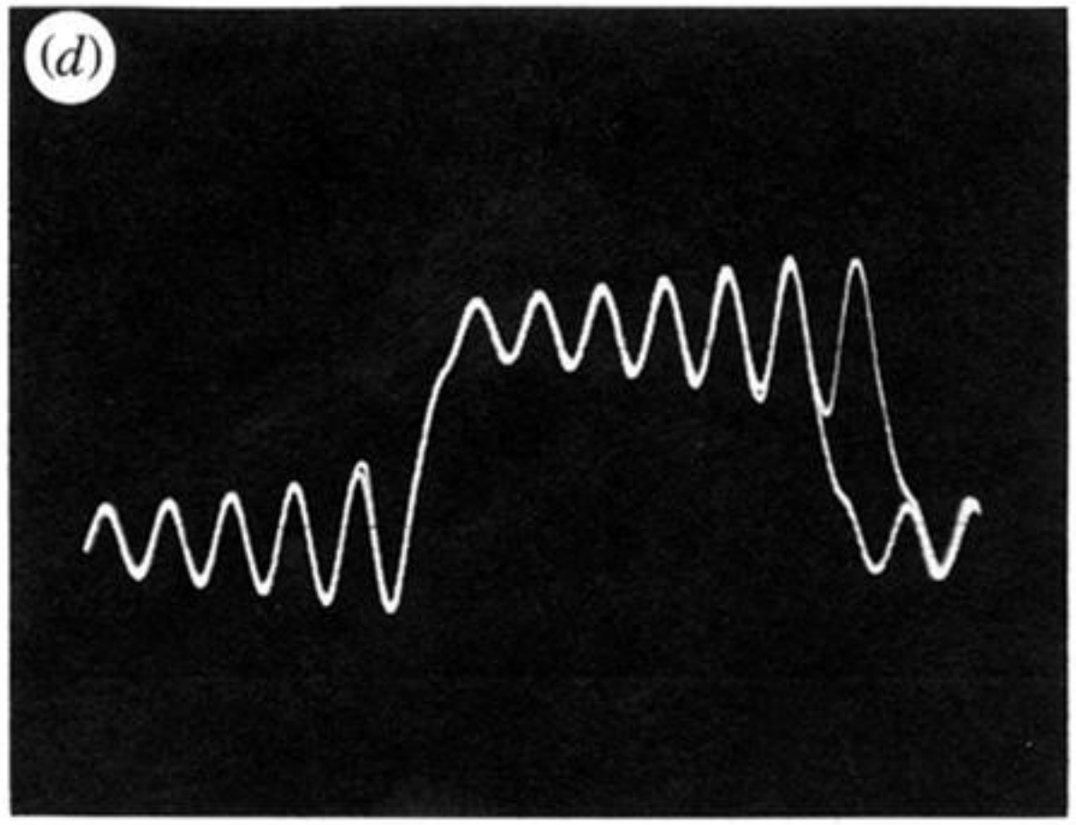

igure 4. Experimental manifestations of chaos in the double-scroll Chua attractor from Chua's scillator ($R = 1800\ \Omega$, $C_1 = 9.4$ nF) (see § 4). (*a*) Two-dimensional projection of the attractor state space; vertical axis: V_1 (1 V/div); horizontal axis: V_2 (200 mV/div). (*b*) Time domain aveforms. Upper trace: $V_1(t)$ (2 V/div); lower trace: $V_2(t)$ (500 mV/div); horizontal axis: t ms/div). (*c*) Power spectrum of $V_2(t)$. Vertical axis: power (dB); horizontal axis: frequency Hz). (*d*) Time domain waveforms showing sensitivity to initial conditions. Vertical axis: $V_1(t)$ V/div); horizontal axis: t (500 μs/div).

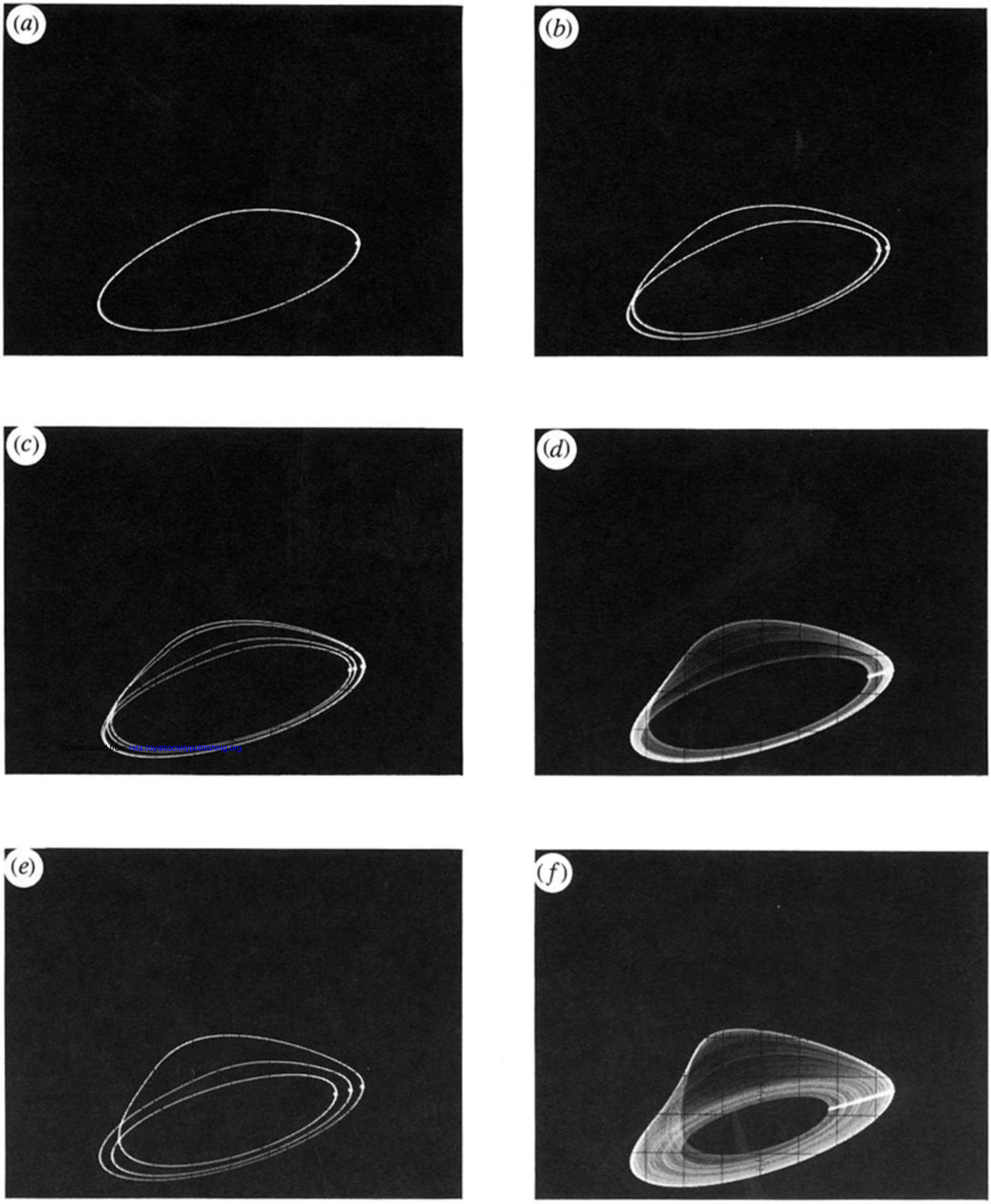

igure 6. Experimental bifurcation sequence for Chua's oscillator showing the period-doubling oute to chaos (a)–(d), a period-three limit cycle in a periodic window (e), and a spiral Chua haotic attractor (f). (a) $C_1 = 10.2$ nF (period-one limit cycle); (b) $C_1 = 9.8$ nF (period-two nit cycle); (c) $C_1 = 9.7$ nF (period-four limit cycle); (d) $C_1 = 9.6$ nF (chaotic attractor with löbius band-like structure); (e) $C_1 = 9.55$ nF (period-three limit cycle); (f) $C_1 = 9.5$ nF (spiral hua chaotic attractor). Horizontal axis: $V_2(t)$ (200 mV/div); Vertical axis: $V_1(t)$ (1 V/div). egative-going intersections of the trajectory through the plane defined by $I_3 = 1.37$ mA are hown highlighted.

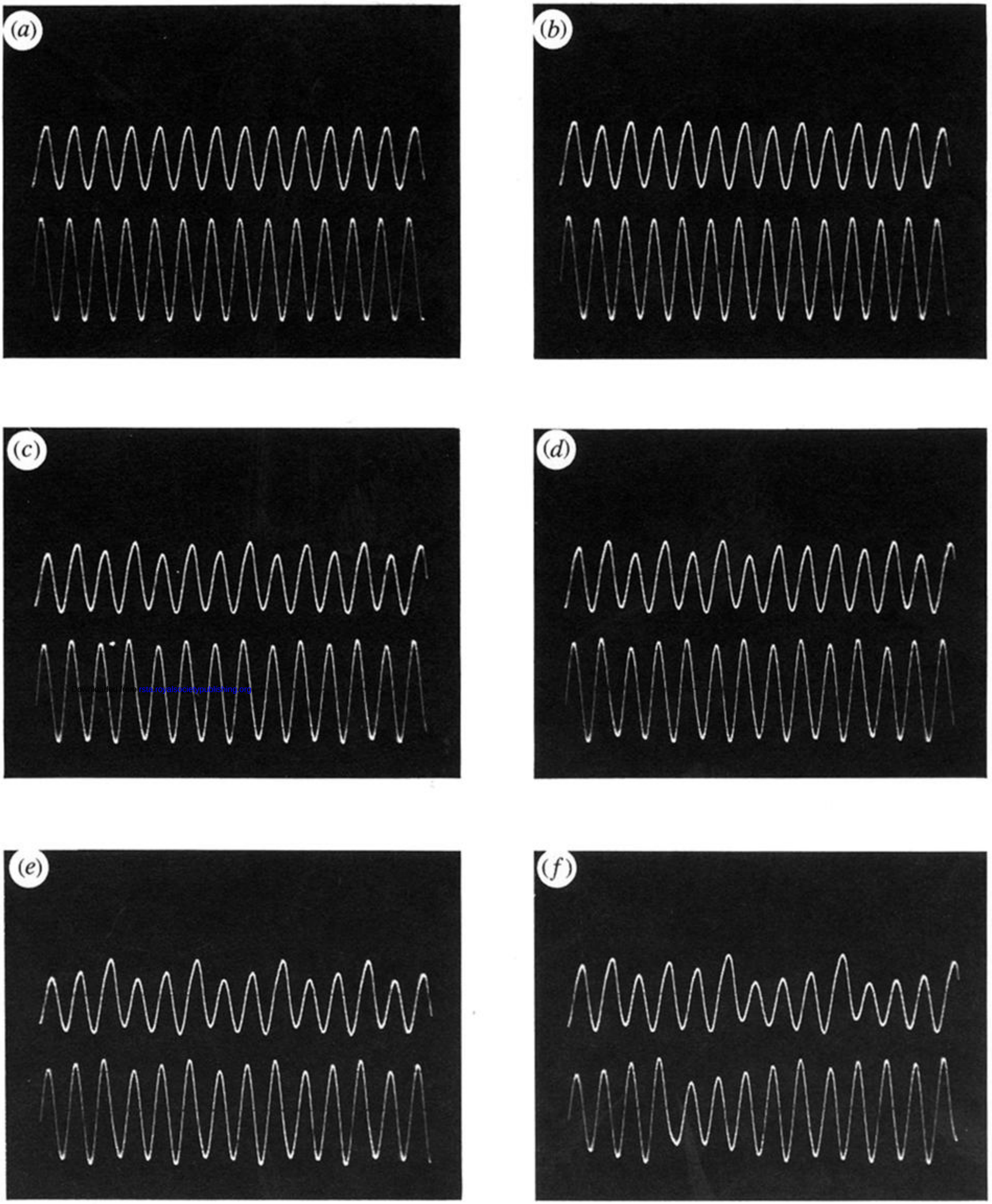

Figure 7. Experimental bifurcation sequence for Chua's oscillator showing period-doubling (*a*)–(*d*), a periodic window (*e*), and spiral Chua chaotic attractor (*f*). Compare with figure 6. (*a*) $C_1 = 10.2$ nF (period-one limit cycle); (*b*) $C_1 = 9.8$ nF (period-two limit cycle); (*c*) $C_1 = 9.7$ nF (period-four limit cycle); (*d*) $C_1 = 9.6$ nF (chaotic attractor with Möbius band-like structure); (*e*) $C_1 = 9.55$ nF (period-three limit cycle); (*f*) $C_1 = 9.5$ nF (spiral Chua chaotic attractor). Upper trace: $V_1(t)$ (2 V/div); Lower trace: $V_2(t)$ (500 mV/div); Horizontal axis: t (500 μs/div).

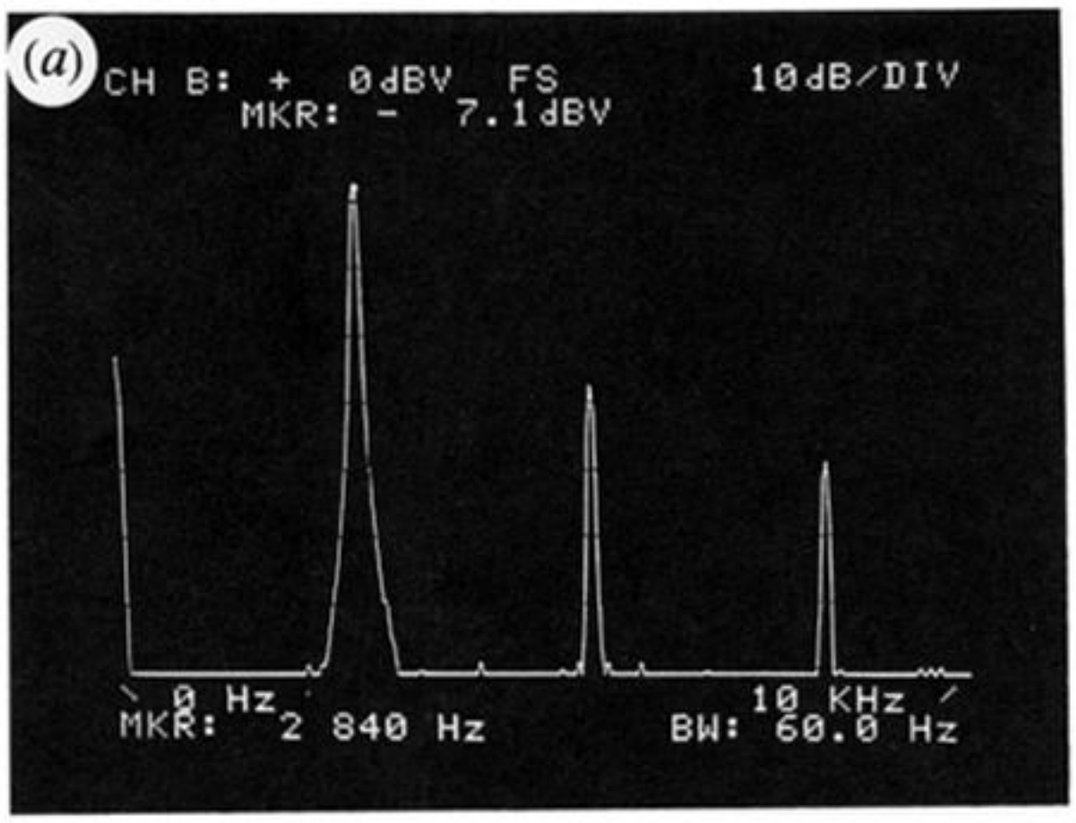

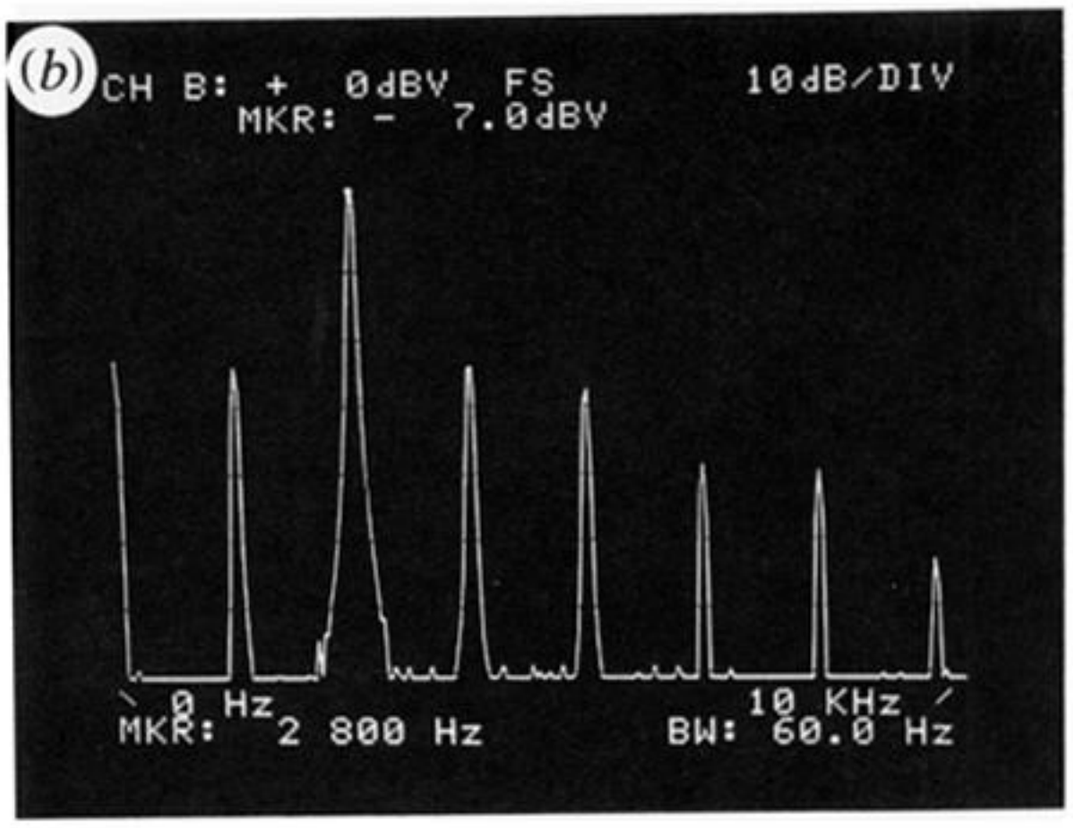

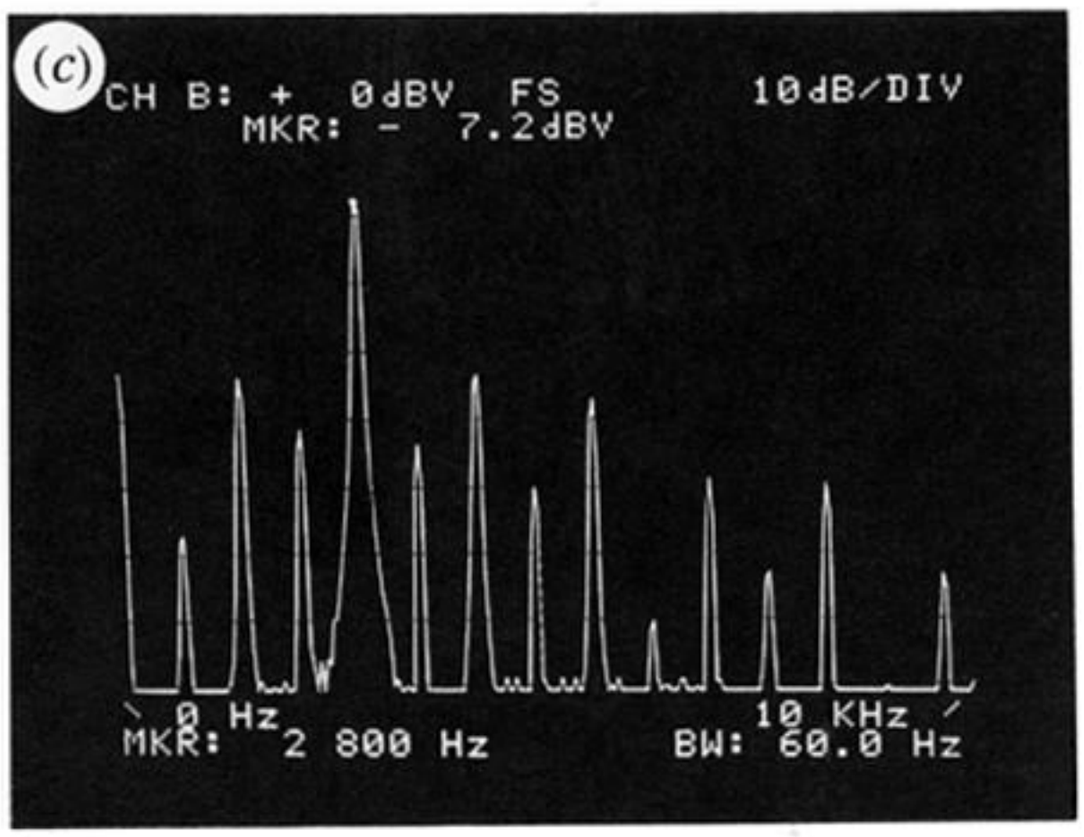

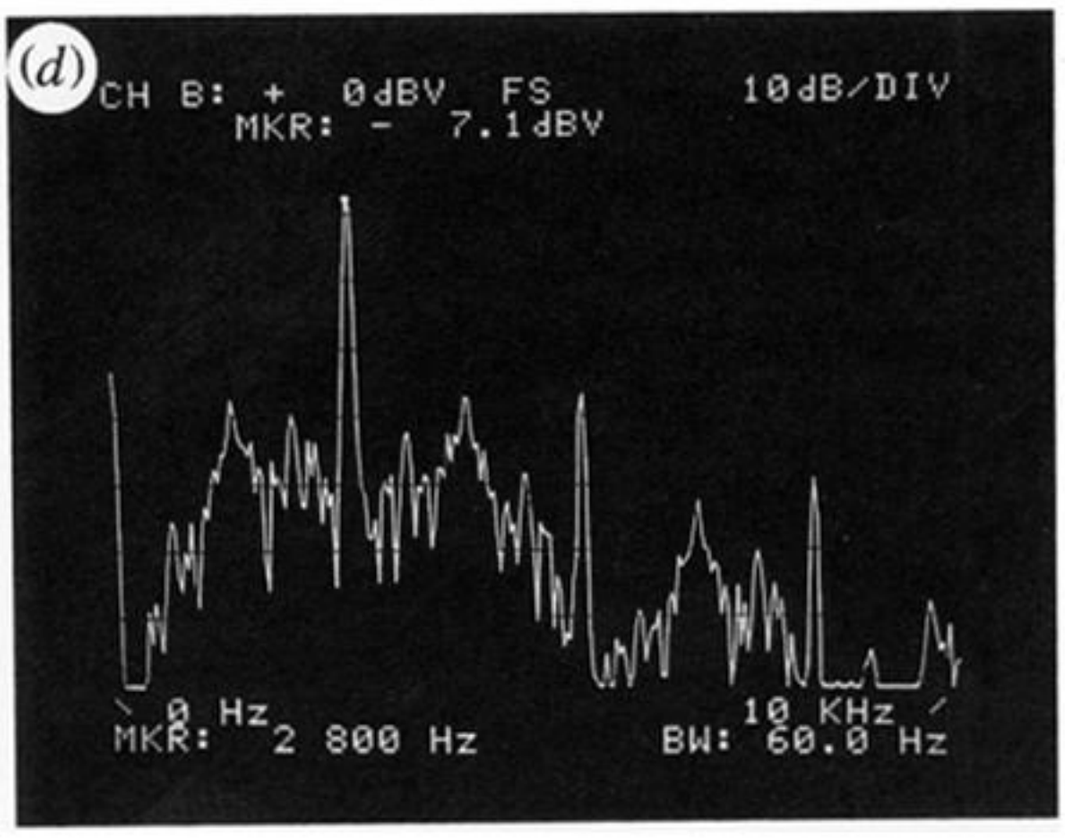

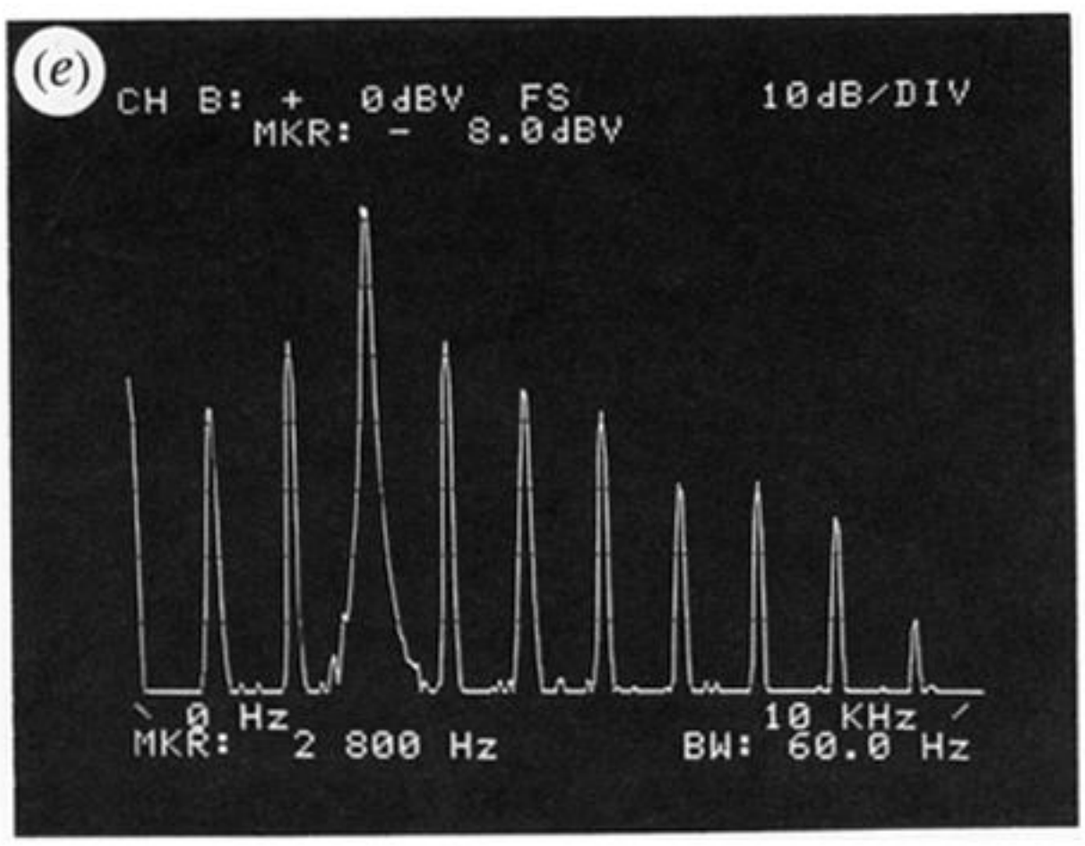

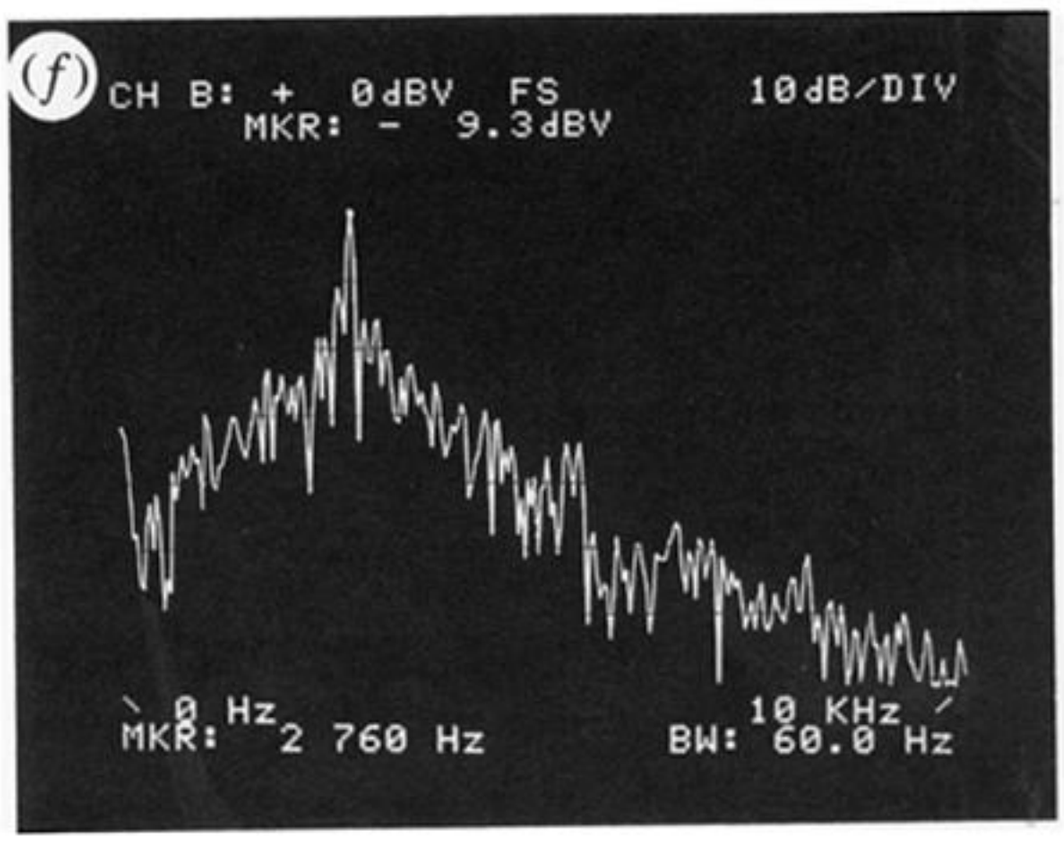

igure 8. Measured power spectra for attractors in Chua's oscillator using an HP3582A Spectrum nalyzer with Hanning window. Compare with figures 6*a*–*f* and 7*a*–*f*. (*a*) Period-one limit cycle, ne power spectrum consists of a fundamental frequency and higher harmonics; (*b*) period-two mit cycle, this periodic signal is characterized by a discrete power spectrum; (*c*) period-four mit cycle, the fundamental frequency is roughly one quarter that of (*a*); signal is characterized y a discrete power spectrum; (*d*) chaotic attractor, the chaotic waveform has a broadband power pectrum but still strong periodicity; (*e*) period-three limit cycle, the fundamental frequency is t approximately one third that of (*a*); (*f*) spiral Chua chaotic attractor, broad spectrum with ttle periodicity evident. Horizontal axis: frequency (kHz); Vertical axis: power (mean squared mplitude of $V_2(t)$) (dB).

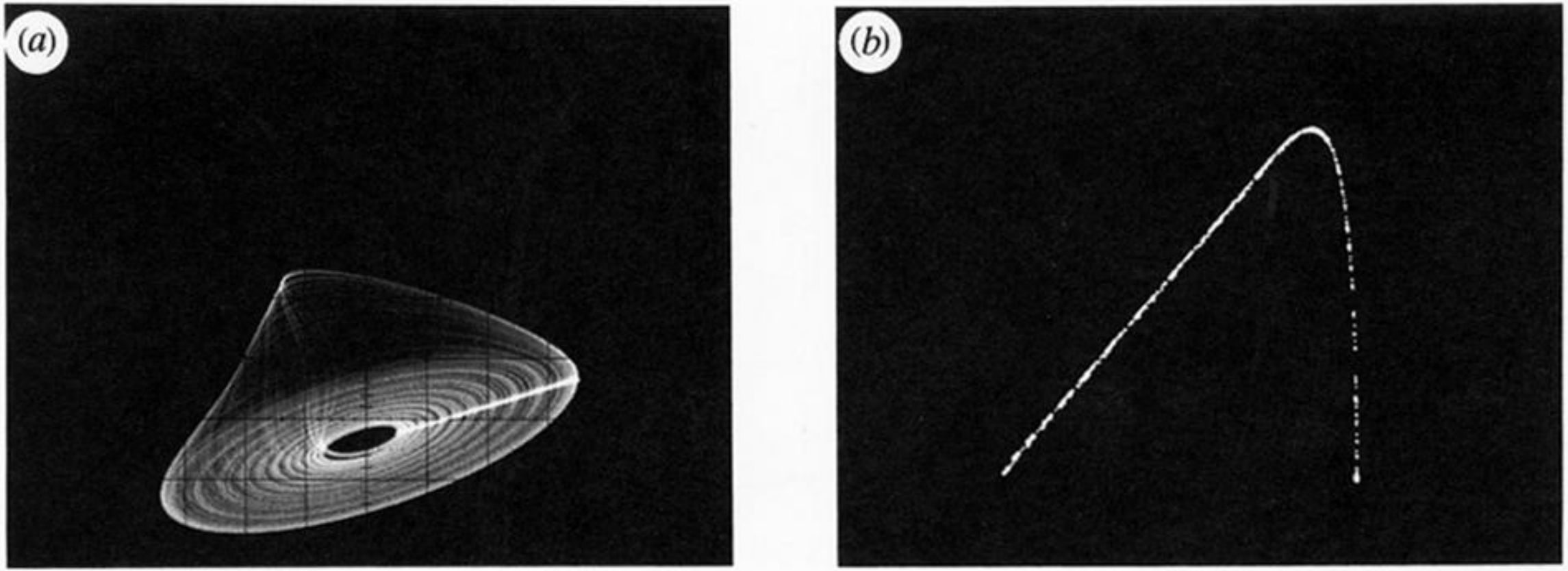

igure 11. (a) Experimental Poincaré section for Chua's oscillator. Horizontal axis: $V_2(t)$ 00 mV/div); vertical axis: $V_1(t)$ (1 V/div). The points of intersection of the trajectory as I_3 ecreases through $I_\Sigma \approx 1.37$ mA are highlighted. (b) Approximate one-dimensional map derived om (a). Horizontal axis: $V_2(t_k)$ (1 V/div); vertical axis: $V_2(t_{k+1})$ (1 V/div).

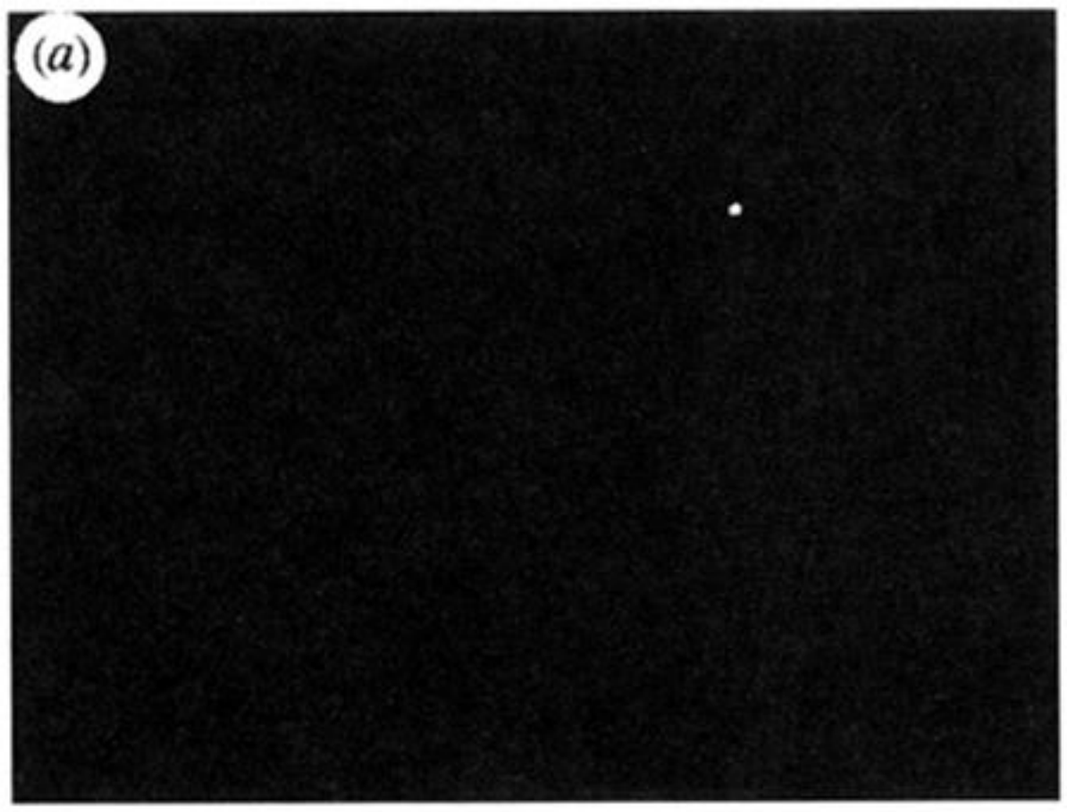

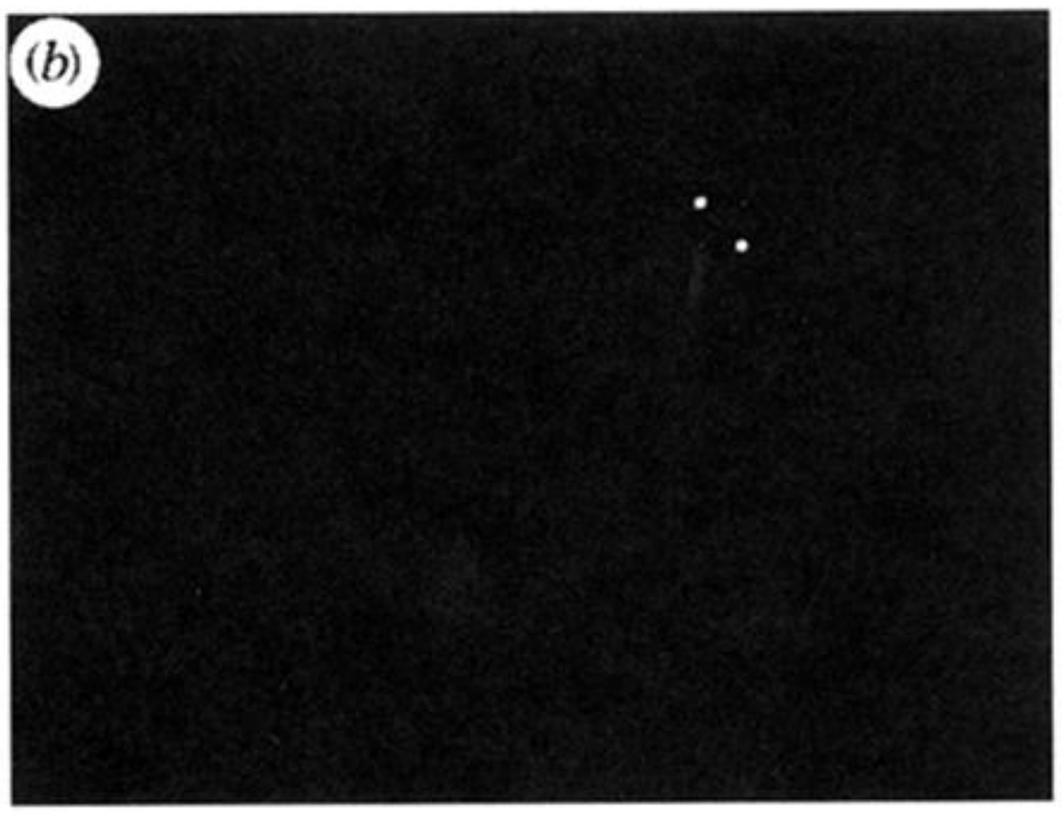

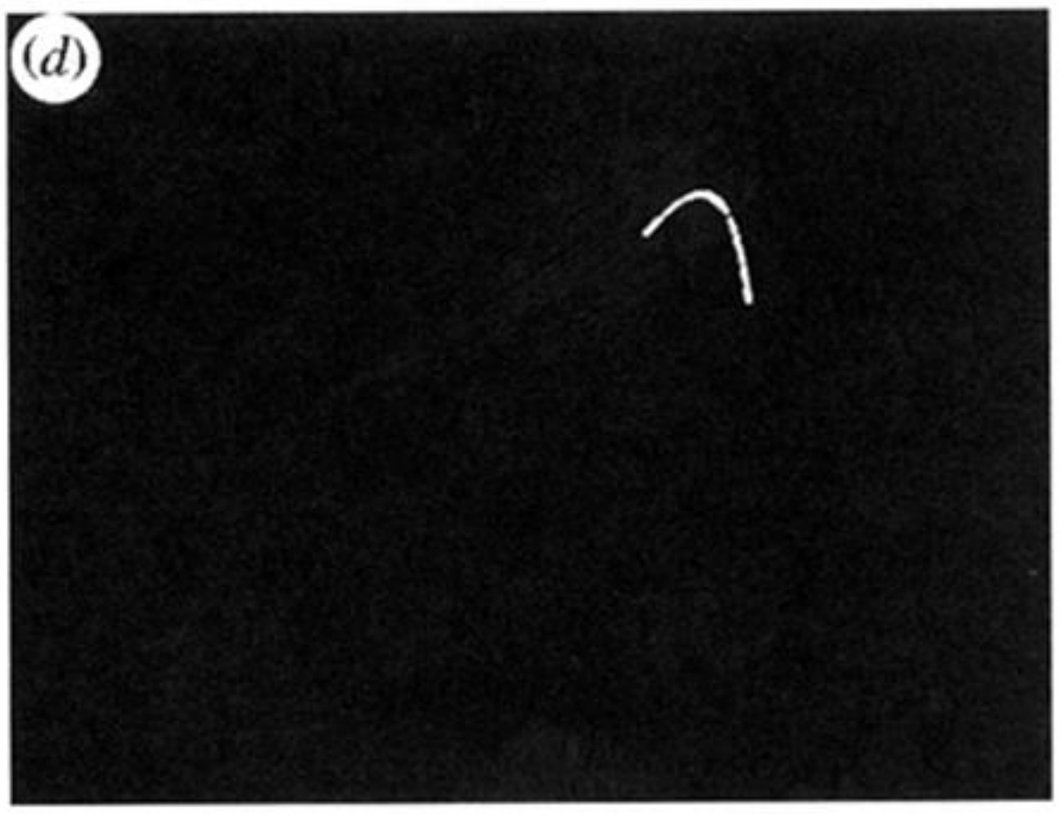

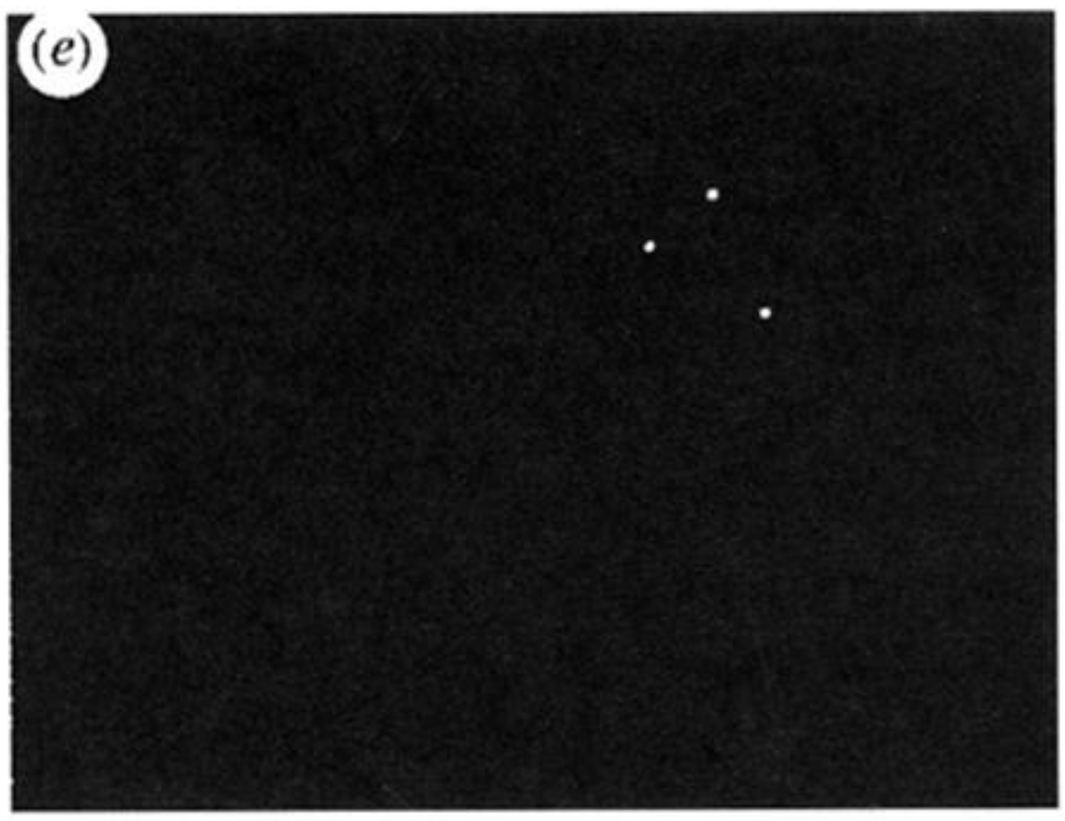

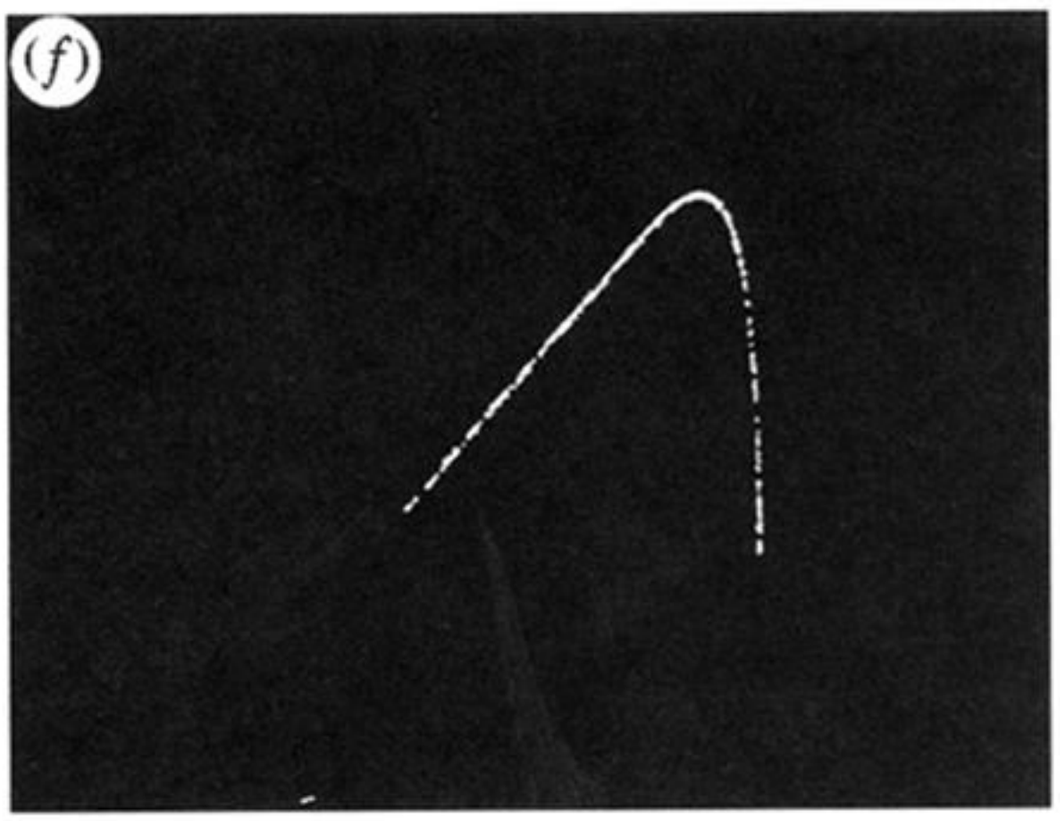

PHILOSOPHICAL TRANSACTIONS OF THE ROYAL SOCIETY A MATHEMATICAL, PHYSICAL & ENGINEERING SCIENCES

Figure 12. Experimental approximate one-dimensional maps for $V_2(t)$ from Chua's oscillator. Compare with figure 6*a*–*f*. (*a*) A period-one limit cycle appears as a fixed point of the approximate Poincaré map, $V_{2k+1} = V_{2k}$; (*b*) period-two limit cycle, $V_{2k+2} = V_{2k}$; (*c*) period-four limit cycle, $V_{2k+4} = V_{2k}$; (*d*) chaotic attractor with Möbius band-like structure, steady-state iterates of the approximate one-dimensional map lie on a unimodal curve; (*e*) period-three limit cycle, $V_{2k+3} = V_{2k}$; (*f*) spiral Chua chaotic attractor, iterates of the approximate one-dimensional map suggest the underlying unimodal shape. Horizontal axis: $V_2(t_k)$ (1 V/div); vertical axis: $V_2(t_{k+1})$ (1 V/div).